A rapid transfer of virions coated with heparan sulfate from the ECM to CD151 defines an early step in the human papillomavirus infection cascade

Annika Massenberg[1], Yahya Homsi[1], Carl Niklas Schneider[1], Snježana Mikuličić[2], Tatjana Döring[2], Luise Florin[2,3,*], Thorsten Lang[1,*]

[1]University of Bonn, Faculty of Mathematics and Natural Sciences, Membrane Biochemistry, Life & Medical Sciences (LIMES) Institute, Carl-Troll-Straße 31, 53115 Bonn, Germany
[2]Institute for Virology, University Medical Center of the Johannes Gutenberg-University Mainz, Obere Zahlbacher Straße 67, 55131 Mainz, Germany
[3] Research Center for Immunotherapy (FZI), University Medical Center of the Johannes Gutenberg-University Mainz, 55131 Mainz, Germany

*Correspondence should be addressed to Thorsten Lang (thorsten.lang@uni-bonn.de) or Luise Florin (lflorin@uni-mainz.de)

Keywords: virus infection, primary attachment site, secondary receptor, filopodia, transport, tetraspanins

Abstract

Human Papillomaviruses (HPVs) are the underlying cause of several types of cancer, albeit they are mostly known for their association with cervical carcinoma. The virions reach their target cells through a break in the epithelial barrier. After binding to heparan sulfate (HS) of the extracellular matrix (ECM), they are recruited via actin-dependent mechanisms to the cell surface where they co-internalize with the entry factor CD151.

The *in vivo* occurring active recruitment from the ECM to the cell surface may be bypassed in cell culture where virions reach the cell surface simply by passive diffusion. To specifically investigate these early events of the infection cascade, we use HaCaT keratinocytes as they produce a robust ECM enabling for abundant virion binding to ECM components such as HS before transfer to cell surface receptors and infection. Employing microscopy, we focus on the basal membrane that for virions is difficult to access by diffusion. We block the active recruitment from ECM attachment sites to the cell body, release the blocking, and monitor the association of virions with CD151 or HS. We observe quick virion recruitment from the ECM to the cell body within 15 min. During recruitment, virions associate with the tetraspanin CD151 present at the cell border or at filopodia. These virions are decorated with HS, which they lose in the next few hours, presumably prior to endocytosis.

37 Our observations reveal a rapid step in the HPV infection cascade: the transfer of HS-coated
38 virions from the ECM to CD151. This step is too fast to account for the asynchronous uptake of HPVs
39 which is likely driven by glycan- and capsid processing.
40
41
42 **Introduction**
43 Already in the 80s, Harald zur Hausen proposed a role of human papillomaviruses in cancer
44 (***zur Hausen, 2009***). Since then, five more classes of oncogenic viruses have been identified (***Galati et***
45 ***al., 2024a***). To date, it is assumed that more than 10% of the worldwide human cancer burden is
46 associated with infectious agents (***Galati et al., 2024a***), from which about a half is caused by
47 *Papillomaviridae* (***Martel et al., 2017***). Thus, the understanding of viral entry strategies has
48 implications going beyond the classical treatment of acute viral infections.
49 Human papillomaviruses are small, non-enveloped viruses with a diameter of ≈55 nm. The
50 icosahedral capsid is mainly composed of pentameric L1 capsomers. Together with fewer L2 capsid
51 proteins, capsomers surround a histone core bearing a circular double-stranded DNA (***Baker et al.,***
52 ***1991; Ozbun and Campos, 2021***). From the more than 200 phylogenetically classified HPV genotypes,
53 the most oncogenic ones are HPV16 and HPV18 (***Galati et al., 2024b***), which are responsible for about
54 70 - 80% of the cervical cancer cases (***Christiansen et al., 2015***). In addition, they cause other severe
55 cancers such as anogenital, head and neck tumors (***Doorbar et al., 2012***).
56 For papillomavirus infection, a disruption of the epithelial barrier is a prerequisite, through
57 which virions reach mitotically active basal cells of the epithelia (***Ozbun, 2019***). Here, virions bind to
58 the linear polysaccharide heparan sulfate (HS) that is present in the extracellular matrix (ECM) and at
59 the plasma membrane surface. HS is covalently linked to proteins forming so called heparan sulfate
60 proteoglycans (HSPGs). Positively charged and polar amino acid residues of the L1 capsid protein form
61 multiple heparan sulfate binding sites that interact with negative charges of HS, resulting in a strong
62 bond (***Dasgupta et al., 2011; Giroglou et al., 2001; Joyce et al., 1999; Knappe et al., 2007; Surviladze***
63 ***et al., 2015***). While in cell culture virions bind to HS on both the cell surface and the ECM, it has been
64 suggested that *in vivo* they bind predominantly to HS of the extracellular basement membrane (***Day***
65 ***and Schelhaas, 2014; Kines et al., 2009; Ozbun and Campos, 2021; Schiller et al., 2010***). In any case,
66 the link between the linear polysaccharide and virions must be disrupted before they can bind to a yet
67 unknown secondary receptor on the cell surface, followed by internalization (***Ozbun and Campos,***
68 ***2021***).
69 The strong electrostatic bonding precludes dissociation as a virion release mechanism. Two
70 alternatives are discussed, that mutually are not exclusive. In the so-called priming model, binding of

71 HS to the capsid results in capsid enlargement and softening (***Feng et al., 2024***), followed by the
72 exposure and cleavage of L1 by kallikrein-8 (KLK8) (***Cerqueira et al., 2015***), exposure of L2 by
73 cyclophilin (***Bienkowska-Haba et al., 2009***), and L2 cleavage by furin (***Richards et al., 2006***). After
74 these structural modifications of the capsid surface the so-called 'primed' virion is able to bind to the
75 secondary receptor. In an alternative model, the HS-virion bond persists. However, heparanases and
76 proteinases cleave HS/HSPGs into fragments. As a result, albeit still bound to the virion surface, the
77 now fragmented HS/HSPG no longer anchors the virion to the ECM (***Surviladze et al., 2012; Surviladze***
78 ***et al., 2015***). Next, released virions may reach cell surface receptors simply by passive diffusion.
79 However, active recruitment is possible as well. For instance, PsVs migrate along actin-rich protrusions
80 from the ECM towards the cell body (***Schelhaas et al., 2008; Smith et al., 2008***). Moreover, cells may
81 reach virions by migrating onto an ECM lawn decorated with virions.

82 While it is generally agreed on that HS is a primary virion attachment site, the molecular
83 identity of the secondary receptor on the main cell body surface is unknown. The secondary receptor
84 complex is most likely of multimeric nature rather than a single molecular component. Possible
85 candidates are proteins known to be crucial for cell entry, as the tetraspanin CD151 (***Mikuličić et al.,***
86 ***2019; Scheffer et al., 2013; Spoden et al., 2008***), integrin-α6 (Itgα6) (***Evander et al., 1997; Yoon et al.,***
87 ***2001***), growth factor receptors (***Mikuličić et al., 2019; Surviladze et al., 2012***), and the annexin A2
88 heterotetramer (***Dziduszko and Ozbun, 2013; Woodham et al., 2012***). From these molecules, the
89 tetraspanin CD151 could play a coordinating role, as tetraspanins organize viral entry platforms in
90 many types of viral infections, including infections with coronavirus, cytomegalovirus, hepatitis C virus,
91 human immunodeficiency virus, human papilloma virus, and influenza virus (***Bruening et al., 2018;***
92 ***Earnest et al., 2015; Florin and Lang, 2018; Hantak et al., 2019; Hochdorfer et al., 2016; Scheffer et***
93 ***al., 2013; Zona et al., 2013***). Such tetraspanin entry platforms could form in a slow and stochastic
94 fashion, which would provide an explanation for the asynchronous virion uptake with half-times of
95 above 10 h (***Becker et al., 2018***). However, it is unclear whether virions associate with CD151 already
96 in the moment of virion transfer from the ECM to the cell surface, or in a subsequent step, e.g. in
97 preparation of endocytosis.

98 Here, we explore the question of a possible link between active virion recruitment to the cell
99 surface and CD151 association. We employ the cell permeable mycotoxin and actin polymerization
100 inhibitor cytochalasin D (CytD). Using a human keratinocyte cell line (HaCaT cells), we find that CytD
101 preserves HPV16 PsVs in the ECM, noticed as PsV accumulations adjacent to the cell periphery. This
102 blocking of the virus transfer is accompanied by co-accumulation of HS in the ECM area. Upon CytD
103 removal, HS-decorated PsVs get from the ECM to the cell body where they associate with CD151. The
104 association of PsVs with CD151 persists within the next few hours, whereas the HS coat is stripped off,

105 and CD151 is observed to agglomerate. These findings distinguish an early step in the infection
106 cascade, the association with CD151 in the moment the virion establishes contact to the cell surface.
107
108
109 **Results**
110 *Cytochalasin D arrests the active recruitment of HPV16 PsVs from the extracellular matrix to the basal*
111 *cell membrane*
112 The molecular surface of PsVs is immunologically indistinguishable from HPV virus particles
113 (***Ozbun and Campos, 2021***), which makes them a widely used tool for studying host cell entry. In this
114 study, we employ HPV16 pseudovirions with an encapsidated luciferase reporter plasmid under the
115 control of the HPV16 promotor (***Wüstenhagen et al., 2018***). Hence, instead of viral DNA a luciferase
116 encoding plasmid enters the cell, enabling the analysis of the infection rate via the luciferase activity.
117 Moreover, the plasmids are composed of nucleotides to which fluorophores can be coupled by click-
118 chemistry. This allows for their microscopic detection by fluorescence microscopy, alternatively to
119 immunolabeling of the L1 capsid protein.
120 PsVs that bind to the ECM at sites distal from the cell body are unable to establish direct
121 contact with entry receptors, until the cell migrates onto them or they are transported along cell
122 protrusions towards the cell body (***Schelhaas et al., 2008; Smith et al., 2008***). Both cell migration and
123 protrusion transport depend on actin dynamics (***Schaks et al., 2019***). We aimed for blocking these
124 active recruitment mechanisms in HaCaT cells, a cell line that is widely used as a cell culture model for
125 HPV infection. They resemble primary keratinocytes in several key aspects: they are not virally
126 transformed and produce large amounts of ECM, promoting interactions between viruses and ECM
127 components and thereby facilitating infection (***Bienkowska-Haba et al., 2018; Gilson et al., 2020***). In
128 addition, subconfluent HaCaT cells form filopodia and filopodial transport is used for the recruitment
129 of ECM-bound virus particles to the cell body *(**Schelhaas et al., 2008, Smith et al., 2008**)*. Together,
130 these features make HaCaT cells a suitable model for studying active PsV recruitment from the ECM
131 to the cell surface.
132 We incubate cells for 5 h with PsVs in the absence or presence of 10 µg/ml (19.7 µM) CytD, a
133 concentration that stops cell migration after a few minutes (***Peng et al., 2011***; using 10 µM CytD).
134 Moreover, in HeLa cells, retrograde transport of virions is sensitive to CytD (2 µM) (***Schelhaas et al.,***
135 ***2008***). Hence, under CytD, active PsV recruitment should be largely inhibited. Frequently, we observe
136 patches of confluent cells which are common to HaCaT cells. Cells at the center of these patches are
137 dismissed during imaging, because hardly any PsVs are bound to their basal membrane, indicating that
138 PsVs do rather not reach this area by passive diffusion. Instead, we focus on isolated HaCaT cells or
139 cells at the periphery of cell patches. At these cells, we find more PsVs per cell than one would expect

140 from the employed ≈ 50 viral genome equivalents (vge) per cell, indicating that PsVs are unequally
141 distributed between the cells. Moreover, in particular after CytD treatment, these PsVs usually are not
142 homogenously distributed around the cell but rather concentrate at one region (Figures 1 to 4). In
143 later experiments (Figures 5 to 8), we investigate the recruitment of PsVs from these regions, defining
144 ROIs for analysis that cover PsVs at the periphery and the cell body (see Supplementary Figures 5A
145 and 8A).

146 In Figure 1, after the 5 h incubation, cells were fixed and stained by a membrane marker, the
147 dye TMA-DPH, to mark the main cell body (Figure 1A, gray lookup table (LUT)). Additionally, PsVs were
148 visualized by click-chemistry (magenta LUT), and HS (cyan LUT) and the membrane protein Itgα6
149 (green LUT) were stained by antibodies. In order to monitor only cell surface events, we stain the cells
150 without prior cell permeabilization (still, fixation perforates the cell membrane to some extent). In the
151 control, PsVs locate strongly in the cell body area (Figure 1A, upper row; see white outline that is based
152 on TMA-DPH staining). In contrast, when CytD was present, the cell body area is largely devoid of PsVs
153 (Figure 1A, lower row; please note that the large central bright area is mainly caused by
154 autofluorescence). Instead, PsVs often accumulate adjacent to the cell body. This adjacent region, that
155 is up to several µm wide and rich in HS, likely includes the ECM. We conclude that upon inhibition of
156 actin-dynamics PsVs do not efficiently reach the basal cell membrane but rather remain accumulated
157 in the ECM area. In contrast, in the control they are actively recruited to the basal cell membrane.
158 Please note that under all conditions PsVs will bind to receptors located outside of the imaged basal
159 membrane, e.g., the entire upper cell membrane, but these PsVs are not visible in the micrographs
160 and therefore not included in the analysis.

161 Comparing in Figure 1A the PsV brightness in the upper (control, magenta LUT) and lower
162 (CytD, magenta LUT) panel suggests that the PsV amounts do not differ greatly. This is surprising, as
163 CytD is not reported to inhibit enzymes involved in capsid modification or HS/HSPGs processing, after
164 which the PsVs supposedly leave the ECM. Provided PsVs processed under CytD would leave the ECM,
165 no major difference in the number of PsVs at the periphery between cells that were treated with or
166 without CytD for 5 h is expected. Therefore, it appears that primed PsVs remain ECM associated. Due
167 to interference from autofluorescence (Figure 1A, large magenta areas in the centers), a quantification
168 of the PsVs with and without CytD is not possible. To study PsVs in the absence of autofluorescence,
169 we employed unroofed cells (***Heuser, 2000***), also referred to as membrane sheets. After pre-
170 treatment of cells as above, membrane sheets are generated by brief ultrasound pulses that remove
171 the upper cellular parts (and thus any intracellular autofluorescence), leaving behind the extracellular
172 matrix and the basal membrane along with the bound PsVs. During imaging, membrane sheets are
173 identified via staining of F-actin with fluorescently labelled phalloidin (Figure 1B, green LUT) that marks

174 the main cell body cortex together with lamellipodia and filopodia. In this experiment we again
175 observe that PsVs, not always but more frequently, after CytD treatment accumulate adjacent to the
176 isolated basal membrane (Figure 1B, magenta LUT, see arrows) that is defined by F-actin staining
177 (Figure 1B, green LUT).

178 The PsV maxima density (Figure 1B, magenta LUT, detected as local maxima of antibody
179 stained L1) and the PsV intensity are quantified in an area covering the cell body and the periphery.
180 Compared to the control, CytD reduces the PsV maxima density by 26% (the PsV maxima density in
181 the control and CytD treated cells is 0.7 and 0.52 PsVs/μm^2, respectively), whereas the maxima
182 intensity increases by 41% (Figure 1C). A histogram of the PsV maxima intensities illustrates that CytD
183 broadens the intensity distribution towards brighter PsVs (Figure 1D, compare black and gray trace).
184 The increase of the PsV intensity after CytD treatment can also be appreciated comparing the upper
185 and middle/lower L1 images in Figure 1B (shown at the same settings of brightness and contrast). As
186 CytD is unlikely to act directly on PsVs (e.g., by fusing them to larger and brighter particles), we assume
187 that the underlying cause of brighter maxima is the resolution limit of the microscope. The densely
188 accumulated PsVs are no longer resolved, overlap, and by this merge to brighter spots. These poorly
189 resolved maxima are on average 41% brighter but of them there are 26% fewer. The decrease in
190 maxima density is in the order of magnitude of the increase in intensity, which yields a roughly similar
191 total signal in both conditions. Hence, active recruitment apparently thins out the PsV accumulations
192 by translocating PsVs from the ECM to the cell body.

193 We addressed whether PsVs would still be accumulated when adding CytD 1 h after the PsVs,
194 rather than adding them simultaneously (Figure 1B, lower panel, CytD after 1 h). As in the CytD
195 condition, accumulated PsVs adjacent to the basal membrane are present more frequently than in the
196 control (Figure 1B, arrows). The PsV maxima intensity distribution (Fig. 1D, green trace) is slightly
197 broader when compared to the control, but narrower than with CytD present for the entire time
198 (Figure 1D), suggesting that PsV binding and recruitment take more than 1 h.

199 Figure 1 indicates that under CytD, when PsVs are not actively collected from the cells, they
200 remain trapped in the ECM next to the cell body. However, for several reasons it cannot be determined
201 exactly how efficient the preservation of accumulated PsVs is. First, our assay is not precise for
202 technical reasons, as the above-mentioned limited resolution results in an underestimation of the
203 number of PsVs the stronger they are accumulated. Second, we do not know how many PsVs in the
204 control are endocytosed during the 5 h of incubation, which is an important number, as adding theses
205 PsVs to the ones being present would be the adequate reference value for comparison to CytD.
206 Moreover, it should be noted that both the degree of PsV accumulation as well as the number of PsVs
207 are highly variable. Even in the control, we occasionally find cells with accumulated PsVs at the

208 periphery, while after CytD we not always encounter accumulated PsVs. This causes a large variability
209 within the data. Still, we consider larger PsV accumulations as a typical effect of CytD incubation
210 (please note that for illustration of this effect we show in the Figures such examples). In any case, we
211 conclude that within the 5 h incubation period with CytD a large fraction of ECM associated PsVs is
212 not able to reach the cell body as in the control, but remains located in its periphery.
213
214 *The blocking of PsV translocation by cytochalasin D is reversible*
215 CytD not only arrests the recruitment of PsVs to the cell body but is known to block other
216 actin-dependent processes, which strongly affects the physiology of the cell. Therefore, we
217 investigated whether PsVs would proceed normally on their infection pathway once CytD is washed
218 off. In order to allow for recovery from CytD, cells were washed after the 5 h PsV/CytD treatment,
219 then incubated for another 19 h and the infection rate was determined by measuring the luciferase
220 activity in the cell lysate. CytD reduced luciferase activity by 29%, as compared to control cells
221 incubated only with PsVs (Figure 1E; left). When PsVs were not washed off after 5 h but left for the
222 entire 24 h incubation, the infection rate increased by 52%, whereas continuous treatment with CytD
223 blocks infection (Figure 1E; right). The latter is in line with previous studies (***Schelhaas et al., 2008;***
224 ***Selinka et al., 2002; Selinka et al., 2007; Spoden et al., 2013***) showing that CytD is a strong inhibitor
225 of HPV infection. In any case, PsVs apparently are able to proceed on the infection pathway upon
226 removal of CytD. The reduced infection rate of 29% can be explained by the 5 h blocking at the
227 beginning of the incubation period that should delay the time course of infection. Altogether, we
228 propose that CytD is suitable for transiently arresting PsVs in a state between primary attachment to
229 HS and cell body receptor binding.
230 Next, we investigated the onset of active PsV recruitment after CytD wash off. Cells were
231 treated with PsVs and CytD for 5 h, washed, and incubated further without PsVs/CytD for 0 min,
232 30 min or 60 min, followed by fixation and staining for PsVs (Figure 2A, magenta LUT) and F-actin
233 (Figure 2A, green LUT). The antibody staining against PsVs, like above the click-chemistry staining, is
234 again highly variable. As a measure of recruitment to the cell body, we calculated the Pearson
235 correlation coefficient (PCC) between PsV-L1 and F-actin staining. The PCC quantifies the similarity
236 between two variables, in this case the pixel values of the two images. The PCC results in the value of
237 1 if images are identical and -1 for an image and its negative. After 5 h of CytD, PsVs often are found
238 accumulated, as seen before, at the edge of the F-actin staining (Figure 2A). The distal PsVs and the F-
239 actin staining partially exclude each other, thus at 0 min we obtain a negative PCC (Figure 2A and D).
240 After 30 min and 60 min, PsVs mostly overlap with F-actin stained areas, which results in positive PCCs

241 (Figure 2A and D). The time course of the change in PCC values suggests an onset of recruitment after
242 CytD removal within 30 min.
243
244 *Confirming in our assay previously proposed steps in HPV infection*
245 As outlined above, PsVs bind tightly to their primary attachment site until the capsid surface
246 undergoes structural changes, which involves modifications of L1 and L2. Consequently, we expect
247 that inhibition of L1 processing during the CytD incubation should inhibit PsV recruitment after CytD
248 removal (Figure 2A and D). To test for this possibility, as employed in earlier studies, the protease
249 inhibitor leupeptin was used to inhibit proteases including KLK8 which is required for L1 cleavage
250 (***Cerqueira et al., 2015***). Employing this inhibitor, the PCC between PsV-L1 and F-actin staining remains
251 negative after CytD removal, showing that for active recruitment indeed the prior action of proteases
252 is a prerequisite (Figure 2B and D). Moreover, the experiment suggests that without PsV priming the
253 PCC between PsV-L1 and F-actin does not increase, for instance, due to cell spreading after CytD
254 removal. In contrast, inhibition of L2 cleavage by a furin specific inhibitor has no effect on the PCC
255 (Figure 2C and D). However, it should be noted that we occasionally observe PsVs not undergoing
256 complete translocation. Instead, they remain accumulated at the border of the F-actin stained area
257 (for example see Figure 2C, 60 min). This results in an increase of the PCC as in complete translocation,
258 explaining why the PCC changes like in the control, despite of a furin effect. Hence, furin may have
259 some effect on a later recruitment step that, however, is undetected in this type of analysis.
260 As outlined above, during the 5 h incubation with CytD, proteases in the ECM are expected to
261 cleave HS chains. These cleavage products should be able to diffuse out of the ECM, unless they remain
262 associated with non-translocating PsVs, present in particular under CytD. Using an antibody that reacts
263 with an epitope present in native heparan sulfate chains, we find that only after CytD and if PsVs were
264 present, the level of HS staining is significantly increased (Figure 3B). As shown in Figure 3A, this
265 stronger HS staining is observed in areas with PsVs (open arrows) and as well in PsV free areas (closed
266 arrows).
267 Next, we used an antibody that reacts with a HS neo-epitope generated by heparitinase-
268 treated heparan sulfate chains (***Yokoyama et al., 1999***; for details see methods). This neo-epitope
269 staining is not affected by CytD and the incubation time (Supplementary Figure 1), suggesting that
270 CytD does not directly affect HS processing. Collectively, our findings indicate that without actin-
271 dependent PsV recruitment HS cleavage products are retained in the ECM, consistent with the
272 hypothesis that cleaved HS remains associated with PsVs (***Ozbun and Campos, 2021***).
273
274 *Fast recruitment of PsVs to the cell body*

275 Next, we studied the time course of PsV recruitment at higher time resolution. Cells were
276 treated as in Figure 1A (in Figure 4, the 0 min time point is identical), followed by removal of
277 PsVs/CytD. Different from Figure 2, we did not calculate the PCC that provides only an approximate
278 idea of the time course, but monitored the diminishment of the integrated density of PsVs locating at
279 the cell periphery, after 0, 15, 30 and 60 min. To delineate the cell periphery from the cell body, the
280 TMA-DPH membrane staining is used as a reference (Figure 4A, the cell periphery is defined by the
281 area enclosed by the two white lines in the PsV-DNA images (magenta LUT)).
282 At 0 min, compared to the control, CytD causes in the periphery a 6-fold increase of PsV signal
283 (Figure 4B). This increase is more than halved when cells were incubated for 15 min, and after 30 min,
284 the level of the control is reached (Figure 4B). This suggests that the half-time of PsV recruitment from
285 the periphery to the cell body is about 15 min. Hence, active recruitment is fast and therefore cannot
286 be a bottleneck in the time course of infection. We conclude that active recruitment is not responsible
287 for the asynchronous virion uptake observed for HPV PsVs.
288
289 *Recruitment of PsVs to CD151*
290 PsVs may approach the entry factor CD151 early, already during recruitment. For studying this
291 possibility, we employ superresolution STED microscopy, analyzing the association of PsVs with CD151
292 over time. Cells are treated and monitored as above, but with an extended time window of up to
293 180 min, as cell surface processes are expected to take longer than an hour. After fixation, PsVs and
294 CD151 were double-stained with antibodies against L1 (Figure 5A, magenta LUT) and CD151 (Figure
295 5A, green LUT). In addition, we stained F-actin with fluorescent labelled phalloidin (shown in
296 Supplementary Figures 2 and 3). We simultaneously image L1 and F-actin in the confocal and CD151
297 in the STED channel.
298 As shown in Figure 5A, CD151 concentrates in spots scattered across the cell surface. It is also
299 present at cell protrusions that are rich in F-actin, and that vary strongly in number and shape
300 (Supplementary Figure 2A shows some examples of these filopodia). Compared to the control, CytD
301 increases the occurrence of accumulated PsVs at the cell periphery, and at early time points PsVs
302 appear brighter (Figure 5A; for overview images and F-actin staining of 0 min/CytD see Supplementary
303 Figure 3A and B; for variability of PsV accumulations after CytD see Supplementary Figure 3B), as
304 already observed in Figure 1B to D.
305 Initially, we wondered whether, after reaching the cell body edge, PsVs are transported
306 quickly further towards the center. Based on the CD151 image, a cell border region was defined (for
307 details see Supplementary Figure 2B). We counted the number of PsVs in this region, and expressed
308 it as percentage of all PsVs in the image. In the control, the fraction of PsVs in the cell border region
309 was rather low, ranging from 13.4% (0 min) to 7.6% (180 min). After CytD, at 0 min, compared to the

310 control the fraction almost tripled (36.5%). It diminished to 16.9% after 60 min, and 12.3% after 180
311 min (Supplementary Figure 2C). This suggests that most PsVs leave the cell periphery within 1 h.
312 The intensity of the CD151 staining between cells is highly variable (Figure 5A and B). In the
313 control, the mean CD151 intensity shows no trend over the 180 min time course, whereas with CytD
314 the intensity after 180 min is diminished in comparison to the control (Figure 5B). The decrease of the
315 CD151 staining intensity points towards the possibility that, after CytD wash off, CD151 is more
316 strongly internalized compared to the control, presumably due to increased co-internalization with
317 endocytosed PsVs. This idea is supported by the observation that, in particular at CytD/180 min, we
318 occasionally observe CD151/PsV agglomerations (Figure 5A, see structures marked by arrows at
319 CytD/180 min, for more examples see Supplementary Figure 4A). We did not study this issue
320 systematically, but some of these structures have clear three-dimensional extension (see
321 Supplementary Figure 4B for axial scans). Therefore, they are likely tubular structures filled with
322 several PsVs, as previously described by electron microscopy (***Schelhaas et al., 2012***). We observe
323 fewer of such structures at control/180 min, probably because cells have been actively interacting
324 with PsVs for altogether 8 h, opposed to 3 h in the CytD treated cells. Hence, after CytD wash off, PsV
325 endocytosis may be more synchronized compared to control, explaining the CD151 staining intensity
326 diminishment at CytD/180 min (Figure 5B).
327 For studying the association between PsVs (L1) and CD151, the PCC between the channels is
328 calculated. The PCCs are around 0.1, with the exception of the 0 min/CytD value that is significantly
329 lower and even negative (Figure 5C, for PCC values of flipped images see Supplementary Figure 5B and
330 C). This reflects the in part mutual exclusion of the two stainings as already discussed above; PsV
331 accumulations tend to be at the cell periphery and the CD151 staining is at the cell body and in
332 filopodia. In any case, the lower PCC at 0 min/CytD suggests that without active recruitment less PsVs
333 reach CD151. At 30 min after CytD, the PCC has reached the level of 0.1 as in the control, which is in
334 line with the idea of fast recruitment as observed in Figure 4. To follow how the basal cell membrane
335 is populated with PsVs over time, as additional analysis we determined the PsVs per μm^2 in ROIs placed
336 in the cell body region. At 0 min, CytD reduces the PsV density to 19 - 33%, albeit the effect is not
337 significant, and at 180 min/CytD the same PsV density as in the control is reached (Supplementary
338 Figure 6A and B). Overall, under CytD there was a trend towards less PsVs present (Supplementary
339 Figure 6A and B). Hence, both Figure 5C and Supplementary Figure 6A and B suggest that active virion
340 transport is required to reach efficiently the basal membrane.
341 We next studied the fraction of PsVs that are closely associated with CD151. As criteria for
342 close association, we define a distance of ≤ 80 nm between PsV and CD151 maxima because this value
343 is close to the resolution limit of the used microscope (***Finke et al., 2020***). In the control, the fraction

344 of PsVs closely associated with CD151 is around 10% (Figure 5D, control), after correction for random
345 background association, for which we used a calibration line based on the same density of PsVs in
346 flipped images (see Supplementary Figure 7). At 0 min after CytD, we start with a fraction of 5.5% of
347 closely associated PsVs, that increases to 12.7% in the next 60 min, although this increase is not
348 significant (Figure 5D, CytD). In any case, it is remarkable that in the absence of active recruitment (0
349 min/CytD) we find half the fraction of closely associates PsVs compared to the control. This indicates
350 that PsVs and CD151 associate very early in the infection cascade, essentially in the moment the PsVs
351 reach the edge of the cell body.
352 In summary, we conclude that within 180 min after a 5 h pre-incubation with PsVs (Figure 5D,
353 control), we encounter a type of steady-state situation (new PsVs are recruited whereas older ones
354 disappear by endocytosis), in which about 10% of the PsVs are associated closely with CD151. CytD
355 diminishes only the PsV-CD151 association at 0 min (5.5%, Figure 5D, CytD), suggesting that PsVs
356 establish contact to CD151 early (see also the increase in the PCC between 0 min/CytD and 30
357 min/CytD, Figure 5C).
358
359 *PsV association with HS*
360 Next, we studied the association between PsVs and HS. As a reference staining for the cell
361 body, we used Itgα6 that is not visible at cell protrusions. PsVs are visualized by click-chemistry and
362 imaged in the confocal channel. HS and Itgα6 were stained by antibodies, and imaged at STED
363 microscopic resolution. The three stainings were simultaneously recorded.
364 As shown in Figure 6A (green LUT), the Itgα6 staining results in a pattern of dense spots. The
365 Itgα6 intensity does not change over time (Supplementary Figure 8E). The pattern of the HS staining
366 (cyan LUT) and the overlap of HS with PsVs and Itgα6 are highly variable (Figure 6A).
367 CytD increases the intensity of HS (Figure 6B; also apparent when comparing the HS brightness
368 in the upper and lower panels of Figure 6A; for an overview of the CytD/0min images see
369 Supplementary Figure 3C). This increase of intensity is particularly notable at the 0 min time point,
370 where the samples treated with CytD have a more than two-fold higher intensity and differ
371 significantly from the control. Hence, in this experiment we reproduce the PsV/CytD mediated HS
372 intensity increase observed in Figure 3B.
373 In the control, the PCC between PsVs and HS are low with no clear trend. The largest PCC is
374 found at CytD/0 min, which reflects the finding that at this time point both PsVs and HS preferentially
375 locate at the cell periphery (Figure 6C, for PCC values of flipped images see Supplementary Figure 8B
376 and C). Over time, the accumulated PsVs diminish due to recruitment, which is accompanied by a PCC
377 approaching zero, as in the control (Figure 6C, 180 min). Additionally, we analyze the PCC between

378 PsVs and HS specifically in the cell body region, excluding the cell periphery (Figure 6D). For the
379 control, the PCC in the cell body region ranges between 0 and 0.05. After CytD, we observe an increase
380 in the PCC from 0 min to 30 min and a decrease from 30 min to 180 min (for PCC values of flipped
381 images see Supplementary Figure 8F and G). When analyzing the PsVs closely associating with HS, at
382 0 min, CytD increases the fraction of PsVs associated with HS more than 3-fold. Over the next 180 min,
383 this fraction gradually decreases until it is equal to the control value (Figure 6E, 180 min).

384 Altogether, the analysis of the PCC between HS and PsVs (Figure 6C) along with the fraction
385 of closely HS associated PsVs (Figure 6E) indicates that CytD treatment increases HS/PsV association
386 at 0 min, likely because PsVs remain accumulated in the ECM. After CytD removal, this association
387 diminishes. An increase in PCC is observed at 30 min specifically in the region of the cell body (Figure
388 6D) which likely reflects the recruitment of HS-coated virions to the cell body. However, as this
389 association diminishes over the subsequent 150 min, an increasing fraction of PsVs is no longer
390 associated with HS due to progressive loss of the HS coat over time, or alternatively, PsVs just may
391 disappear after internalization.

392 Next, for each PsV we plot the 'distance to the next nearest Itgα6 maximum' against 'the
393 distance to the next nearest HS maximum' (Figure 7). In the control, the distances remain essentially
394 unchanged over the entire observation time; 59% - 65% of the PsVs are at a short distance (< 250 nm)
395 to both Itgα6 and HS (Figure 7B, black; see also Supplementary Table 1), 12 - 15% are at a short
396 distance (< 250 nm) to HS but not to Itgα6 (> 250 nm) (Figure 7B, green; see also dashed green box in
397 Figure 9 marking PsVs in the ECM). Regarding the distance plots of untreated cells in Figure 7 (please
398 compare the upper distance plots from left to right), they suggest that the distance patterns do not
399 change over the 180 min observation time. In cells treated with CytD, a larger fraction of PsVs is
400 accumulated at the periphery at the 0 min time point, which is reflected in a larger fraction (46% as
401 opposed to 12% in the control; Figure 7B, green; Supplementary Table 1) of PsVs with a short distance
402 (< 250 nm) to HS but not to Itgα6. In the distance plots, it can be noticed that the PsVs in the CytD
403 treated cells over time acquire shorter distances to Itgα6 and larger distances to HS (Figure 7C, lower
404 row). The population with short distances to HS and large ones to Itgα6 strongly diminishes from 46%
405 to 11% (Figure 7B, CytD, green). After 180 min, the distances are similar to the untreated control.
406 Between CytD/60 min and CytD/180 min, the fraction of PsVs with a large distance (> 250 nm) to HS
407 and a short distance (< 250 nm) to Itgα6, representing PsVs at the cell body without HS (see also
408 dashed magenta box in Figure 9), increases from 9.6% to 25.2% (Figure 7B, magenta). This is
409 inconsistent with the idea of endocytosis of HS-coated PsVs that would only diminish short distances
410 to Itgα6 but not create long distances to HS, which is what we observe. The observation supports the

411 idea that PsVs lose their HS coat after translocating to the cell surface, which is in line with the
412 transient increase in the cell body PCC between HS and PsVs at 30 min (Figure 6D).

413 The recruitment of HS towards the cell body after removal of CytD, which indirectly
414 demonstrates that PsVs are coated with HS, is suggested by a shortening of the HS-Itgα6 distance over
415 180 min only after CytD wash off (Supplementary Figure 8D). Together with the observation that the
416 PCC between PsVs and HS in the cell body area increases (Figure 6D), the data suggest that HS-coated
417 PsVs are recruited to the cell body. A fraction of PsVs sheds HS within one hour after removing CytD
418 (Figure 7C, lower panels, showing increasing PsV-HS distances after 60 min). This is the time window
419 in which we notice the occurrence of endocytic PsV/CD151 structures (see above and Supplementary
420 Figure 4B).

421 Actin retrograde transport underlies the filopodial virion transport and is the integrative result
422 of three components (***Smith et al., 2008; Schelhaas et al., 2008***). On the one side, actin filaments in
423 the cell periphery are pushed into the cell body area when actin polymerizes at their tips. The
424 retrograde filament movement causes tension and is facilitated by F-actin degradation opposed to the
425 side of F-actin growth. Moreover, the motor protein myosin II exerts force on actin filaments, pulling
426 those towards the cell body. As CytD broadly interferes with F-actin dependent processes like
427 filopodial transport and cell migration, we investigated the effects upon inhibition of only one
428 component of actin retrograde flow, namely the myosin II mediated retrograde movement towards
429 the cell body. Instead of CytD, we employed in the 5 h preincubation the myosin II inhibitor
430 blebbistatin (***Schelhaas et al., 2008***). For the control (0 min), we show in Figure 8A one example of a
431 cell with comparatively many PsVs at the periphery (as mentioned above, the PsV pattern is highly
432 variable and also in the control we occasionally observe PsV accumulations) to better illustrate the
433 difference to the PsV pattern occasionally seen with blebbistatin. After blebbistatin treatment (0 min),
434 PsVs do not reach the central cell body as in the control, but are less dispersed than after CytD
435 treatment, seemingly as if recruitment started but stopped in the midst of the pathway (Figure 8A,
436 blebbistatin). The PCC between PsVs and HS, like after CytD (Figure 6C), is elevated after blebbistatin,
437 albeit the effect is not significant (Figure 8C). The cell body PCC is not, as under CytD, at 30 min (Figure
438 6D) but already at 0 min elevated (compare Figure 6D to Figure 8D), which can be explained by partial
439 recruitment. This is further supported by the fact that only 8% of PsVs are closely associated with HS
440 (Figure 8E; blebbistatin, 0 min) compared to 15% after CytD treatment (Figure 6E; 0 min). Furthermore,
441 after 0 min PsV incubation with blebbistatin we observe no effect on the HS intensity (compare Figure
442 8B to Figure 3B and Figure 6B). Hence, in contrast to CytD, blebbistatin does not preserve the PsVs in
443 the ECM where they associate with HS, but ongoing actin polymerization may push actin filaments
444 along with PsVs towards the cell body.

445

446 *PsV binding in the absence of a diffusion barrier*

447 Throughout all experiments, we observe at 0 min/CytD only few PsVs at the basal membrane
448 (Figure 1A, Supplementary Figure 6A and B; see also PCC at 0 min between PsVs an CD151 in Figure
449 5C), suggesting that in the absence of active recruitment the access to the basal membrane via passive
450 diffusion is limited. We wondered, how many PsVs may bind to the cell membrane without a diffusion
451 barrier? For this reason, we incubated EDTA detached HaCaT cells in suspension with PsVs for 1 h at 4
452 °C, followed by re-attachment for 1 h. Under these conditions, we find, despite of a shorter incubation
453 time (1 h versus 5 h), a roughly 3-fold larger PsV density (1.7 PsVs/μm^2 (Supplementary Figure 6D))
454 than the highest density observed in the other experiments. However, it should be noted that values
455 of the different experiments cannot be directly compared. Aside from the different treatments,
456 another difference lies in the size of the imaged membrane. The re-attachment of cells is not complete
457 after 1 h (compare size of adhered membranes in Supplementary Figure 6A and 1A), wherefore the
458 membranes are likely strongly ruffled, which results in the underestimation of the membrane area. As
459 a result, we overestimate the PsVs per μm^2 adhered membrane (please note that we cannot re-attach
460 cells for longer times as we then lose PsVs due to endocytosis). In any case, the experiment suggests
461 that PsVs bind more efficiently to membrane surface receptors without a diffusion barrier. We
462 conclude that in our assay PsVs cannot readily bypass the active PsV recruitment by diffusing directly
463 to the basal cell membrane, which is plausible, because to make this happen a 55 nm large PsV must
464 diffuse through the narrow gap between glass-coverslip and adhered cell.

465

466

467 **Discussion**

468 In this study, we investigate the early events in HPV16 infection occurring at the cell surface.
469 Our findings reveal that in our assay actin dependent mechanisms, rather than passive virion diffusion,
470 are crucial for recruiting HS-coated virus particles from the adhesive ECM to the basal cell membrane.
471 PsVs associate early with CD151, and shed their HS-coat before endocytosis. Moreover, we propose
472 that reversible blocking of active recruitment by CytD allows for a more synchronized observation of
473 the steps on the cell surface.

474

475 *A reversible CytD blocking of PsV recruitment from the ECM to the basal cell membrane*

476 Many viruses use cell surface HS for primary attachment, including herpes simplex virus
477 type 1, human cytomegalovirus, human immunodeficiency virus type 1, adenovirus type 2, dengue
478 virus, hepatitis B virus, and vaccinia virus (***Cagno et al., 2019; Giroglou et al., 2001; Tian et al., 2021***).

479 HPVs could be different as they bind as well to HS of the extracellular basement membrane, at least
480 *in vivo* during the wounding and healing processes required for infection (***Day and Schelhaas, 2014;***
481 ***Kines et al., 2009; Ozbun and Campos, 2021; Schiller et al., 2010***).
482 By treating cells with CytD, we block actin-mediated recruitment, leading to a 6-fold
483 accumulation of PsVs at the cell periphery after 5 hours (Figure 4B). After CytD removal, infectivity is
484 reduced by 29% (Figure 1E). Some reduction is to be expected, as PsVs have ≈20% less time to
485 complete infection as compared to cells that were not treated with CytD. Hence, the infection assay
486 suggests that the treatment is largely reversible and only slightly harmful, if at all. However, the
487 luciferase infection assay does not distinguish between actively recruited PsVs and PsVs that bind
488 passively by diffusion to the upper membrane. The latter fraction likely dominates the total infection
489 rate and should be less affected by CytD than the fraction of actively recruited PsVs. Therefore, if the
490 infection pathway of a small fraction of actively recruited PsVs is irreversibly inhibited, we may not be
491 able to detect this effect on the background of unaffected passively binding PsV.
492 Upon CytD washout, PsVs approach the basal membrane with a half-time of ≈15 minutes, as
493 suggested by the diminishment of accumulated PsVs at the periphery (Figure 4B). The half-time could
494 be longer if cell spreading is also underlying the translocation of PsVs onto the cell body. However, we
495 assume that this is rather unlikely, as cell spreading would increase the PCC between PsVs and F-actin
496 under a condition where PsVs are not-primed (and therefore not actively recruited) but cell spreading
497 occurs, which is not the case in Figure 2B and D (CytD/leupeptin).
498 In Figure 4, we observe fast diminishment of the peripheral PsVs within 15 min. It is in principle
499 possible that after CytD removal ECM-accumulated PsVs are merely washed off. However, after only
500 15 min, the effect of this could not have been very strong, considering the still 6-fold accumulation of
501 PsVs after the 5 h incubation with CytD.
502 Furthermore, CytD pre-treatment appears to synchronize uptake: We observe endocytic
503 structures after CytD treatment more frequently and the CD151 intensity diminishes over time only
504 after the CytD treatment (Figure 5B). We estimate that, compared to control, about 6-fold more PsVs
505 (Figure 4B) approach the cell surface in a coordinated fashion after CytD removal, which likely
506 enhances the number of endocytic events compared to untreated cells. We therefore propose that
507 the processing of the PsVs in the ECM is contributing to desynchronization and is largely completed
508 after the 5 h pre-incubation with CytD.
509
510 *The role of actin-driven virion transport*
511 The strong electrostatic interaction between HPV and HS implies that some processing — via
512 HS cleavage or structural capsid changes — is a prerequisite for the release of virions from the ECM.

513 CytD likely does not inhibit HS processing (***Jamieson et al., 2021***) nor is it likely to inhibit KLK8.
514 Therefore, we assume that, although PsVs are primed after 5 h of incubation with CytD, they remain
515 in the ECM. They may be associated via weaker interactions, and actin-driven transport is required for
516 pulling the HS-coated virions out of the sticky matrix towards the cell body. Sticky PsV aggregations
517 that are released from HeLa cell surface after binding and blocking of the subsequent entry pathway
518 have been observed earlier and might reflect similar HS/PsV-stuctures (***Mikuličić et al., 2025***). It is
519 possible that an ECM bound virion is not exposed to all required processing factors at the same time.
520 In this case, migration through the ECM enables for contact with all processing enzymes. Once the
521 fully processed virions have reached the cell surface, detachment from the ECM may be facilitated by
522 new bonds established between the PsVs and cell surface receptors. Now, the PsVs and cell surface
523 receptors move towards the center of the cell body by intracellular dynamics which results in CD151
524 accumulation at virus binding sites (see Figure 5 as well as Supplementary Figure 4) and ultimately
525 endocytosis.

526 Both CytD and blebbistatin increase PsV-HS colocalization, but blebbistatin allows partial
527 recruitment (compare Figure 6C and Figure 8C as well as Figure 6D and Figure 8D), indicating that actin
528 retrograde flow initiates movement, while myosin II contributes to sustained transport. As a result,
529 virus movement can proceed to some extent after blebbistatin treatment. However, the subsequent
530 blocking of transport at later time points reflects the inhibition of myosin II, which eventually disrupts
531 the cytoskeletal dynamics and force generation that is necessary for sustained transport. In contrast,
532 CytD directly interferes with actin polymerization, leading to an earlier and more persistent blocking
533 of virus transport due to structural disruption of the filopodial tracks themselves.

534 Altogether, our findings support earlier reports showing that HPV utilizes filopodia for cell
535 entry, migrating at several micrometers per minute (***Schelhaas et al., 2008; Smith et al., 2008***). This
536 translocation is fast compared to the entire infection process and therefore cannot largely contribute
537 to the asynchronous HPV uptake.

538 The analyzed PsVs hardly bind to the basal cell surface directly by diffusion (Supplementary
539 Figure 6, compare PsV maxima density at 0 min/CytD in A and B to C). Therefore, the actin-driven
540 virion transport would play a decisive role in HPV infection if cells would form a monolayer with a
541 disruption at which ECM is present and that is approached by PsVs, a scenario similar to *in vivo*
542 infection. In addition, cell migration could establish contact between PsVs and the cell surface.

543

544 *HaCaT cells as model system in HPV infection*

545 Inhibition of HPV16 PsV transport diminishes infection only of subconfluent but not of
546 confluent HaCaT cells by about 50% (***Schelhaas et al., 2008***). Therefore, actin-dependent translocation

547 along protrusions may be dispensable for infection at a high cell density (***Schelhaas et al., 2008***) and
548 merely increases the exposure of cells to virions (***Smith et al., 2008***) that can readily bind to the upper
549 cell membrane. We are not aware of a PsV translocation mechanism from the upper to the basal
550 membrane. Therefore, in our assay, PsVs bound to the upper membrane are not expected to show up
551 at the basal membrane. Comparing 0 min of control and CytD (Supplementary Figure 6A and B), we
552 find that compared to the control 19 - 33% of the PsVs reach the basal membrane in the absence of
553 active transport, or in other words, most likely by passive diffusion. Actually, the range from 19 – 33%
554 must be a strong overestimate as PsVs in the control are in transit and many actively recruited PsVs
555 are already internalized during the 5 h incubation period. For this reason, we propose that most likely
556 much less than 10% of the PsVs reach the basal membrane by diffusion. Moreover, in the absence of
557 the diffusion barrier, the density of bound PsVs is strongly increased (Supplementary Figure 6D),
558 showing indirectly that at the basal membrane the binding sites are difficult to access without active
559 recruitment. Taken together, we propose the large majority of PsVs analyzed in our assay are ECM
560 bound and actively recruited to the basal cell membrane.
561 The increased virion exposure via active recruitment could be relevant *in vivo*, as wounding of
562 the epidermis results in upregulation of filopodia formation (***Vasioukhin et al., 2000***). Filopodia usage
563 not only facilitates infection but also increases the likelihood of virions to reach their target cells during
564 wound healing, namely the filopodia-rich basal dividing cells. In fact, several types of viruses exploit
565 filopodia during virus entry (***Chang et al., 2016***), hinting at the possibility that for HPV and other types
566 of viruses actin-driven virion transport may play a more important role than it is currently assumed.
567 In this scenario, sub-confluent HaCaT cells, or even better single HaCaT cells, would be an ideal model
568 system for the microscopic study of these very early infection steps that involve ECM attachment and
569 subsequent active recruitment, as supposed to occur during *in vivo* infection of basal keratinocytes
570 after binding of virions to the basement membrane (***Bienkowska-Haba et al., 2018; Day and***
571 ***Schelhaas, 2014; Kines et al., 2009; Schiller et al., 2010***). In contrast, in biochemical infection assays,
572 virions diffusing to HSPGs on the cell surface, and by this bypassing active recruitment, are assayed
573 together with the actively recruited virions. Should cells secrete little ECM and are grown to
574 confluency, the passively binding virions are supposed to strongly dominate the infection rate in a
575 biochemical infection assay.
576
577 *Recruited PsVs are decorated with HS which they lose over time*
578 CytD treatment increases the HS signal when PsVs are present (Figure 3B and 6B). A
579 relationship between PsVs and HS cleavage products has been previously suggested (***Ozbun and***
580 ***Campos, 2021; Surviladze et al., 2012***), and we propose that our data is in line with these previous

581 observations. It should be noted that under conditions without the 5 h CytD blocking, PsVs may only
582 briefly reside in the ECM and as a result are less decorated with HS. Hence, under our assay conditions
583 the HS decoration of virions may be enhanced in comparison to other assays.

584 At the 0 min time point post-CytD, 15% of the PsVs are closely associated with HS, but this
585 fraction declines to 4.3% within 180 min (Figure 6E). Considering the important role of HS as a primary
586 attachment site, the fraction of 15% appears unexpectedly small. There are multiple possible
587 explanations for underestimating the number of PsVs closely associated with HS. One factor may be
588 that accumulated PsVs are not well-resolved (see above), which results in an underestimation of HS
589 associated PsVs in particular at CytD/0 min. Other explanations include that the HS antibody does not
590 reach all HS epitopes in the dense matrix. Yet another explanation could be that PsV binding to HS and
591 antibody binding to HS is sometimes mutually exclusive, a hypothesis which is supported by data
592 showing that the HPV capsid possesses multiple HS binding sites (***Dasgupta et al., 2011; Richards et***
593 ***al., 2013***). Finally, not all PsVs bound to the ECM are expected to bind to HS but could also bind to
594 laminin 332 (***Culp et al., 2006***). Together, our data suggests that PsVs initially are recruited with HS
595 attached to them and then shed it, potentially either upon receptor binding or further capsid
596 rearrangement. These observations are in line with a previous study showing reduced HS
597 colocalization during productive infection (***Selinka et al., 2007***).

598 The initial HS-coat may facilitate the formation of a complex with PsVs and cell surface
599 receptors such as integrins or growth factor receptors (GFRs) (***Ballut et al., 2013; Pellegrini, 2001***).
600 This could facilitate receptor clustering and engagement as shown previously for coronavirus infection
601 (***Bugatti et al., 2025; Clausen et al., 2020; Zhang et al., 2023***), as well as the binding of signaling
602 molecules to the cell surface (***Miladinova et al., 2022***). Here, CD151 may support receptor clustering
603 by binding to both integrins and GFRs (***Hemler, 2005; Mikuličić et al., 2019***). In addition, earlier studies
604 suggested that cofactors like laminin-332 and growth factors further stabilize these interactions (***Culp***
605 ***et al., 2006; Mikuličić et al., 2019; Richards et al., 2014; Surviladze et al., 2012***). Furthermore, the
606 HPV capsid has multiple binding sites for distinct functions (***Richards et al., 2013***) which supports the
607 idea that HS fulfills several roles during viral entry — first by promoting capsid attachment, then
608 inducing conformational changes, and finally by assisting in receptor engagement and clustering.
609 However, HS cleavage alone is not sufficient for ECM release; active transport and capsid priming
610 remain essential (see leupeptin effect in Figure 2B and D).

611

612 *PsV-CD151 association occurs early at the cell surface*

613 CD151 is a known mediator of HPV entry (***Scheffer et al., 2013; Spoden et al., 2008***). Our data
614 shows that about 10% of the PsVs are closely associated with CD151 at all time points. This fraction is

615 lower at 0 min post-CytD (Figure 5D, see also lower PCC in Figure 5C), indicating that actin disruption
616 impairs initial CD151 engagement. Hence, the data suggest that PsVs establish contact to CD151
617 assemblies already during recruitment to the cell surface, and from then on, the fraction of closely
618 associated PsVs remains constant. At first glance this implies that, after the initial formation of the
619 PsV-CD151 assemblies, they do not change in nature. However, we observe agglomerated CD151
620 maxima (locally patched maxima) close to PsVs at later time points that likely are endocytic structures
621 (see arrow in Figure 5A and Supplementary Figure 4). This agglomeration process is not detected in
622 our analysis as we only determine the next nearest CD151 maximum. Some further CD151
623 reorganization into larger entry platforms has been previously observed (***Florin and Lang, 2018***). This
624 is in accordance with the observation that virions enter the cell in crowds with many of them
625 occupying one endocytic organelle (***Schelhaas et al., 2012***).
626 For the PsVs closely associated with CD151, one may have expected a larger fraction than
627 10%. Given that PsVs are not supposed to bind directly to CD151 and that CD151 is likely part of a
628 larger membrane structure, like a tetraspanin enriched microdomain, our ≤ 80 nm distance criteria
629 may be too short and by this we underestimate the associated fraction. Altogether, we propose that
630 an early contact between PsVs and the cell surface involves CD151 (Figure 9).
631
632 *Integration of our data into the HPV infection cascade*
633 HPV infection is the result of several steps, starting with the initial binding of virions via
634 electrostatic and polar interactions (***Dasgupta et al., 2011***) to the primary attachment site HS
635 (***Richards et al., 2013***), which induces capsid modification (***Cerqueira et al., 2015; Feng et al., 2024***)
636 and HS cleavage (***Surviladze et al., 2015***), enabling the virion to be released from the ECM or the
637 glycocalyx. Next, virions bind to the cell surface to a secondary receptor complex that forms over time,
638 and become internalized via endocytosis, before they are trafficked to the nucleus (***Mikuličić et al.,***
639 ***2021; Ozbun and Campos, 2021***). Regarding the transition from the primary attachment site to cell
640 surface receptor binding, as already outlined in the introduction, two models are discussed. In one
641 model, proteases cleave the capsid proteins. After priming, the capsids are structurally modified and
642 the virion can dissociate from its HS attachment site. It has been suggested that capsid priming is
643 mediated by KLK8 (***Cerqueira et al., 2015***) and furin (***Richards et al., 2006***). In our system, KLK8
644 inhibition blocks PsV transport, while furin inhibition has some effect that, however, cannot be
645 detected in this analysis (Figure 2D) suggesting furin engagement at later steps in the infection
646 cascade. This is in line with earlier *in vitro* studies on the role of cell surface furin (***Day et al., 2008;***
647 ***Day and Schiller, 2009; Surviladze et al., 2015***). In any case, our results align with both models of ECM

648 detachment: one involving HS cleavage (HS co-transfer) and another one involving capsid modification
649 (by e.g., KLK8).
650 We propose that after 5 h of CytD treatment, glycan-induced structural activation as well as
651 capsid processing by proteases such as KLK8 of the capsid and HS cleavage essentially are completed
652 ((i) in Figure 9). Subsequently, the HS decorated virion is recruited from the ECM to the basal cell
653 membrane, which takes about 15 min. In a time window of 30 min after CytD wash off (ii), PsV-CD151
654 association occurs. (iii) In the samples recorded 30 – 180 min after CytD wash off, we observe that
655 PsVs lose their HS-coat, and individual PsV-CD151 assemblies seem to merge into larger structures
656 that are subsequently endocytosed. This model highlights the role of ECM interactions, actin
657 dynamics, and receptor engagement in HPV16 entry.
658
659
660 **Materials and Methods**
661 *Antibodies and PsVs*
662 We used the following primary antibodies in immunostainings of proteins. For the capsid
663 protein L1, a rabbit polyclonal antibody (pAb) K75 (diluted 1:1000) as described previously (***Knappe et***
664 ***al., 2007; Rommel et al., 2005***), for CD151 a mouse monoclonal antibody (mAb) (1:200) (Biorad, cat#
665 MCA1856GA), and for Itgα6 a rabbit polyclonal antibody (1:200) (Invitrogen, cat# PA5-12334) were
666 used. For Heparan sulfate (HS) a mouse IgM monoclonal antibody (1:200) (amsbio, cat# 370255-S) was
667 used that reacts with an epitope in native heparan sulfate chains and not with hyaluronate,
668 chondroitin or DNA, and poorly with heparin (mAb 10E4 (***David et al., 1992***)). For HS neo-epitope
669 (***Yokoyama et al., 1999***) detection, a mouse monoclonal antibody (1:200) (amsbio, cat#370260-S) was
670 used that reacts only with heparitinase-treated heparan sulfate chains, proteoglycans, or tissue
671 sections, and not with heparinase treated HSPGs. The antibody recognizes desaturated uronic acid
672 residues (mAb 3G10 (***David et al., 1992***)). As secondary antibodies we used a STAR GREEN-coupled
673 goat-anti-rabbit (1:200) (Abberior, cat# STGREEN-1002-500UG), an AlexaFluor 594-coupled donkey-
674 anti-rabbit (1:200) (Invitrogen, cat# A21207), an AlexaFluor 594-coupled donkey-anti-mouse (1:200)
675 (Invitrogen, cat# A21203), an AlexaFluor 594-coupled donkey-anti-mouse IgM (1:200) (Invitrogen,
676 cat# A21044), a STAR RED-coupled goat-anti-mouse (1:200) (Abberior, cat# STRED-1001-500UG) and
677 a STAR RED-coupled goat-anti-rabbit (1:200) (Abberior, cat# STRED-1002-500UG). Additionally,
678 phalloidin iFluor488 (1:1000 of ready to use solution) (abcam, cat# ab176753) or phalloidin iFluor647
679 (1:1000) (abcam, cat# ab176759) was used to stain F-actin. Staining of the PsV plasmid DNA was
680 performed by click-labeling according to the manufacturer's instructions with the dye 6-FAM Azide
681 (Baseclick EdU 488 kit, Carl Roth, cat# 1Y67.1).

682 HPV16 PsVs were produced following established procedures (***Buck et al., 2004; Spoden et***
683 ***al., 2012***). HEK293TT cells were cultured in 175 cm² flasks and transfected with polyethylenimine (PEI),
684 using equimolar amounts of codon-optimized HPV16 L1/L2 (pShell-16L1wt-16L2wt) and a reporter
685 plasmid (pGL4.20-puro-HPV16 LCR (***Wüstenhagen et al., 2018***)). For the production of 5-ethynyl-2'-
686 deoxyuridine (EdU)-labeled PsVs, the culture medium was replaced 5 hours post-transfection with
687 fresh medium containing 30 µM EdU. After 48 hours, cells were harvested, centrifuged, and washed
688 twice with phosphate-buffered saline (PBS) supplemented with 9.5 mM $MgCl_2$ (1x PBS/ $MgCl_2$). After
689 the final centrifugation, the pellet was resuspended in 1x PBS/ $MgCl_2$ containing 0.5% Brij58 (Sigma-
690 Aldrich), and 250 units Benzonase (Merck Millipore), and incubated at 37°C for 24 hours on a rotating
691 platform. Subsequently, lysates were chilled on ice and the NaCl concentration was adjusted to 0.85
692 M. After clarification by centrifugation, the supernatant was loaded onto an iodixanol (Optiprep)
693 gradient consisting of 39%, 33%, and 27% layers (bottom to top). Gradients were equilibrated for 90
694 minutes at room temperature before ultracentrifugation at 55,000 rpm for 3.5 hours at 16°C. Fifteen
695 fractions of 300 µl each were collected from the top and analyzed via luciferase reporter assay to
696 identify peak fractions. PsV titers were determined based on packaged genomes (viral genome
697 equivalents, vge) as previously described (***Spoden et al., 2012***). The concentrations of stock solutions
698 were 7.7 x 10^6 vge/µl (for microscopy experiments) and 14.1 x 10^6 vge/µl (for the luciferase assay).
699
700 *Cell culture*
701 For microscopy, human immortalized keratinocytes (HaCaTs) (Cell Lines Services, Eppelheim,
702 Germany) were cultured in high glucose Dulbecco's modified Eagle's medium (DMEM + GlutaMAX,
703 Gibco, cat# 61965-026) supplemented with 10% FBS (PAN Biotech, cat# P30-3031) and 1%
704 Penicillin/Streptomycin (10,000 U/ml Penicillin, 10 mg/ml Streptomycin; PAN Biotech, cat# P06-
705 07100) at 37 °C with 5% CO_2. For the luciferase infection assay, cells were grown at 37°C and 5% CO_2
706 in Dulbecco's modified Eagle's medium (DMEM + GlutaMAX, Thermo Fisher Scientific), supplemented
707 with 10% FBS (Sigma-Aldrich), 1% minimum essential medium non-essential amino acids (MEM non-
708 essential amino acids (Thermo Fisher Scientific)), and 5 µg/ml ciprofloxacin (Fresenius Kabi). For
709 experiments, the antibiotics in the medium were omitted.
710
711 *Sample preparation and immunostaining*
712 About 150,000 HaCaT cells were plated onto 25 mm diameter poly-L-lysine (PLL) coated
713 (100 µg/ml PLL for 30 min) glass coverslips in 6-well plates and incubated for 24 h at 37°C and 5% CO_2.
714 The next day, cells were incubated at 37°C and 5% CO_2 for 5 h with PsVs (46 vge/plated cell) and
715 10 µg/ml cytochalasin D (CytD; stock solution 10 mg/ml in dimethyl sulfoxide (DMSO)) (Life

716 Technologies, cat# PHZ1063) or 30 µM (−)-blebbistatin (stock solution 13.68 mM in DMSO) (Sigma-
717 Aldrich, cat# B0560-1MG) in DMEM supplemented with 10% FBS. For controls, we added the same
718 amount of DMSO without CytD or blebbistatin. Cells were washed with PBS (137 mM NaCl, 2.7 mM
719 KCl, 1.76 mM KH_2PO_4, 10 mM Na_2HPO_4, pH 7.4) and fresh DMEM supplemented with 10% FBS was
720 added. Cells were incubated further at 37°C and 5% CO_2 for 0 min (here the medium was added
721 followed by immediate removal), 15 min, 30 min, 60 min and 180 min.

722 In another set of experiments, about 150,000 HaCaT cells were plated onto 25 mm diameter
723 PLL coated glass coverslips in 6-well plates and incubated for 24 h at 37°C and 5% CO_2. The next day,
724 cells were incubated at 37°C and 5% CO_2 for 5 h with PsVs (46 vge/plated cell) and 10 µg/ml CytD
725 either together with 100 µM leupeptin (stock solution 100 mM in ddH_2O) (Carl Roth, cat# CN33.1) or
726 5 µM Furin inhibitor I (stock solution 5 mM in DMSO) (Sigma-Aldrich, cat# 344930-1MG) in DMEM
727 supplemented with 10% FBS. For controls, we used only 10 µg/ml CytD. Cells were washed with PBS
728 and fresh DMEM supplemented with 10% FBS was added. Cells were incubated further at 37°C and
729 5% CO_2 for 0 min, 30 min and 60 min.

730 To analyze PsV binding to detached HaCaT cells, about 350,000 HaCaT cells per well were
731 plated in 6-well plates and incubated for 24 h at 37°C and 5% CO_2. The next day, cells were detached
732 by a 15 min incubation with 10 mM EDTA (in PBS, pH 7.4) at 37°C and 5% CO_2. Detached cells were
733 collected and incubated with 46 vge/cell in DMEM supplemented with 10% FBS under constant
734 rotation at 4 °C for 1 h. Cells were washed three times with PBS at 4 °C to remove any unbound PsVs.
735 Then, cells were seeded onto 25 mm diameter PLL coated glass coverslips in 6-well plates and
736 incubated for 1 h at 37°C and 5% CO_2.

737 Before staining, cells were washed twice with PBS and fixed at room temperature (RT) with
738 4% PFA in PBS for 30 min, unless membrane sheets were generated. In this case, the coverslips were
739 placed in ice cold sonication buffer (120 mM KGlu, 20 mM KAc, 10 mM EGTA, 20 mM HEPES, pH 7.2)
740 and a 100 ms ultrasound pulse at 100% power was applied. This was repeated until in total about 10
741 pulses were applied at different locations of the coverslip. Then, membrane sheets were fixed like
742 cells at RT with 4% PFA in PBS for 30 min. PFA was removed, and residual PFA was quenched by 50 mM
743 NH_4Cl in PBS for 30 min. Afterwards, samples were blocked with 3% BSA in PBS for 30 min. Staining of
744 PsVs was performed by click-labeling with the dye 6-FAM for 30 min at RT according to the
745 manufacturer's instructions. Then, samples were washed three times with PBS. In case of no PsV
746 labeling by click-chemistry, directly after blocking, the respective primary antibodies were added:
747 mouse IgM mAb against HS (1:200), mouse mAb against Δ-HS (1:200), rabbit pAb against Itgα6 (1:200),
748 mouse mAb against CD151 (1:200) and rabbit pAb K75 against L1 (1:1000) in 3% BSA in PBS for 2 h.
749 Samples were washed three times with PBS before adding the respective secondary antibodies and

750 fluorescent labelled phalloidins in 3% BSA in PBS for 1 h: for HS we added AlexaFluor 594 coupled to
751 donkey-anti-mouse IgM (1:200), for Δ-HS AlexaFluor 594 coupled to donkey-anti-mouse (1:200), for
752 Itgα6 STAR RED coupled to goat-anti-rabbit (1:200), for CD151 AlexaFluor 594 coupled to donkey-anti-
753 mouse (1:200) or STAR RED coupled to goat-anti-mouse (1:200), for L1 AlexaFluor 594 coupled to
754 donkey-anti-rabbit (1:200) or STAR GREEN coupled to goat-anti-rabbit (1:200) and for F-actin
755 phalloidin iFluor488 (1:1000) or phalloidin iFluor647 (1:1000). Afterwards, samples were washed three
756 times with PBS, followed by mounting of the coverslips onto microscopy slides using ProLong Gold
757 antifade mounting medium (Invitrogen, cat# P36930).
758
759 *Confocal and STED microscopy*
760 For confocal and STED microscopy, samples were imaged employing a 4-channel STED
761 microscope from Abberior Instruments (available at the superresolution light microscopy facility of
762 the LIMES institute, Bonn, Germany). The microscope is based on an Olympus IX83 confocal
763 microscope equipped with an UPlanSApo 100x (1.4 NA) objective (Olympus, Tokyo, Japan). Confocal
764 and STED micrographs were recorded simultaneously. For confocal imaging, a 488 nm laser was used
765 for the excitation of 6-FAM, STAR GREEN and phalloidin iFluor488, and emission was detected at 500–
766 550 nm. For STED imaging, a 561 nm laser (at 45%) was used for the excitation of AlexaFluor 594
767 (detection at 580–630 nm) and a 640 nm laser (at 45%) for the excitation of STAR RED and iFluor647-
768 labelled phalloidin (detection at 650-720 nm), in combination with a 775 nm laser for depletion (at
769 45%). The pixel size was set to 25 nm, for overview images a pixel size of 250 nm was used.
770
771 *Analysis of confocal and STED micrographs*
772 Images were analyzed using Fiji ImageJ (***Schindelin et al., 2012***) in combination with a custom
773 written macro, essentially as described previously (***Schmidt et al., 2024***). When analyzing double
774 stainings of Alexa594 (red channel) and STAR RED (long red channel), we corrected for crosstalk from
775 the red into the long red channel by subtracting 40% of the intensity of the red channel image from
776 the long red channel image.
777 First, images were smoothed with a Gaussian blur to improve maxima detection. For confocal
778 PsV-DNA micrographs, we employed a Gaussian blur of $\sigma = 1$, and for confocal PsV-L1 and STED
779 micrographs a Gaussian blur of $\sigma = 0.5$. Local maxima were detected using the 'Find Maxima' function
780 (noise tolerance 60 for L1 if stained together with phalloidin iFluor488, and 80 if stained together with
781 CD151, HS, or phalloidin iFluor647, 3 for click-labeled PsVs, 8 for CD151, 6 for HS and 15 for Itgα6),
782 yielding maxima positions in pixel positions. For analysis, regions of interest (ROIs) were defined (for
783 details see figure legends).

784 In order to define the cell border region (Supplementary Figure 3B), the ImageJ 'Make Binary'
785 function was used on CD151 STED micrographs for generating a binary mask. When possible, the
786 'Wand' tool was used to further outline the area covered by the cell, otherwise the same was done
787 manually using the original micrograph as a reference. From the outline in the binary mask, a ROI was
788 created, that was then filled in white with the 'Flood Fill' Tool. The ROI was shrunk to a 20-pixel broad
789 strip, and cleared outside of the strip, what leaves a 20-pixel broad, closed ribbon marking the
790 intracellular side of the cell border that, however, exhibits arbitrary edges produced in the process
791 above. These edges were removed by manual adjustments with the 'Pencil' tool and the clear
792 function. Afterwards, the ROI defines the intracellular side of the cell border. The ROI was
793 symmetrically broadened by 40 pixels (using the 'Enlarge' function). From the now at least 60 pixels
794 broad ROI, approximately two thirds covered the intracellular and one third the extracellular side. In
795 this ROI, using the ImageJ 'Find Maxima' function, PsV-L1 maxima were detected (at a noise tolerance
796 of 80) with a custom written macro in ImageJ both in the cell border region ROI and in a ROI covering
797 the entire micrograph (excluding a 2-pixel edge). From these values, the percentage of PsVs within the
798 cell border region was calculated.
799 For measuring intensity over time, we measured in the ROI the mean gray value. For
800 background correction, we subtracted the mean gray value measured in a ROI next to the cell.
801 For measuring maxima intensity, a ROI with a diameter of 125 nm (5 pixels) was placed onto
802 the determined maxima positions (see above). Using these ROIs, the average mean gray value of each
803 maximum was measured. The average background mean gray value was measured in a ROI placed
804 next to the cell and subtracted from the average mean gray value of the maxima. For each membrane
805 sheet, the average maxima intensity was calculated, followed by averaging of the values of the
806 membrane sheets.
807 To measure the shortest distance, e.g., between PsV and CD151 maxima, as a quality control
808 for the PsV maxima (CD151 maxima do not undergo the quality control step) we placed onto each
809 maximum position a horizontal and a vertical linescan (31 pixels long × 3 pixels width). Afterwards, we
810 fitted a Gaussian distribution to the intensity distribution of each maximum. Only if at least one of the
811 fits exhibits a fit quality of $R^2 > 0.8$ and if the Gaussian maximum located central to the intensity
812 distribution the maximum was included in the further analysis. Moreover, using a 125 nm ROI at the
813 PsV and CD151 maxima positions, the center of mass of fluorescence was determined, yielding the
814 maxima positions in sub-pixels. Based on these positions we further calculated the shortest distance
815 of a PsV maximum to the nearest CD151 maximum.
816 Using the shortest distances, we either calculated the fraction of closely associated PsVs (PsVs
817 with a distance ≤ 80 nm to e.g., CD151) over time, or the average shortest distance over time. The

818 fraction of closely associated PsVs was corrected for random background association that increases
819 with the maxima density. The relationship between background association and maxima density was
820 expressed by a linear equation obtained from the same images re-analyzed after flipping them
821 horizontally and vertically (see e.g., Supplementary Figure 7).
822 The Pearson correlation coefficient (PCC) was calculated with a custom written macro in
823 ImageJ. As a control, we performed the analysis on horizontally and vertically flipped ROI-defined
824 images as well (see e.g., Supplementary Figure 5A). The cell body PCC between PsVs and HS is
825 measured in smaller ROIs covering exclusively the cell body region (this is confirmed with the Itgα6 or
826 F-actin image as reference).
827 Per condition and biological replicate, 14 - 15 images were analyzed and values were
828 averaged. For images from one set of experiments, in the figure the same channels are shown at the
829 same settings of brightness and contrast, if not stated otherwise.
830
831 *Epi-fluorescence microscopy and image analysis*
832 For epifluorescence microscopy, we used microscopic equipment and settings as previously
833 described (***Homsi et al., 2014***) except of the illumination system, which was replaced by a SPECTRA X
834 Light engine; Lumencor, Beaverton, OR, USA). In brief, PFA-fixed cells were imaged in a chamber filled
835 with 1 ml of PBS to which 50 µl of a saturated solution of TMA-DPH [1-(4-tri-methyl-ammonium-
836 phenyl)-6-phenyl-1,3,5-hexatriene-p-toluenesulfonate (T204; Thermofisher)] in PBS was added, for
837 visualizing the membranes in the blue channel. PsVs, HS and Itgα6 were imaged in the green, red and
838 far-red channels, respectively.
839 For analysis, rectangular ROIs of ≈ 45 x 10^3 pixel were placed onto the cell body such that
840 approximately one half of the ROI covers the ECM area and the other one the cell body. The cell
841 periphery was defined using the TMA-DPH image from which a binary mask was created. With
842 reference to the binary mask, a band of up to 30 pixels width was created beginning at the cell body
843 and reaching out towards the cell periphery. Using this ROI, in the PsV-DNA image the size of the ROI
844 and the mean gray values were measured from which the integrated intensities were calculated after
845 background correction.
846
847 *Luciferase infection assay*
848 HaCaT cells were grown in 24-well plates and allowed to adhere overnight. The following day,
849 cells were treated with HPV16 PsVs at a concentration of approximately 100 vge per cell, in the
850 presence or absence of 10 µg/ml cytochalasin D (CytD) in DMSO or an equivalent amount of DMSO
851 (Control). In one condition, PsVs/CytD were applied for 5 hours, after which the medium was replaced

852 with fresh medium lacking the compounds, and incubation was continued for additional 19 hours (in
853 total 24 h). In another condition, cells were exposed to PsVs/CytD continuously for the full 24 h period.
854 Then, cells were washed with PBS and lysed using 1 x Cell Culture Lysis Reagent (Promega, cat# E153A).
855 Following high-speed centrifugation, luciferase activity in the cleared lysates was quantified using an
856 LB 942 Tristar 3 Multimode Microplate Reader (Berthold Technologies). Cytotoxic effects,
857 accompanied by a loss of membrane integrity (indicated by released lactate dehydrogenase (LDH)),
858 were determined by measuring the LDH levels in the cell lysates. LDH activity was assessed using the
859 CytoTox-ONE Homogeneous Membrane Integrity Assay (Promega, cat# G7891). LDH fluorescence was
860 quantified according to the manufacturer's instructions using the LB 942 Tristar 3 Multimode
861 Microplate Reader.
862
863 *Statistics*
864 Microscopy data sets were based on three biological replicates. One replicate includes per
865 time point the average of 14 - 15 images analyzed (with exception of Figure 4, which includes 14 – 35
866 analyzed cells per replicate and time point). For the infection assay, data sets were based on three
867 biological replicates. One biological replicate is the average of three technical replicates. Data was
868 tested for significance with a two-tailed, unpaired student's *t*-test with significance * = $p < 0.05$,
869 ** = $p < 0.01$ and *** = $p < 0.001$.
870
871
872 **Acknowledgement**
873 LF and TL were funded by the Deutsche Forschungsgemeinschaft (DFG, German Research Foundation),
874 Projektnummer 322863883 (LF and TL) and Projektnummer 270976260 (TL). This publication was
875 supported by the Open Access Publication Fund of the University of Bonn.
876
877
878 References
879 **Baker TS**, Newcomb WW, Olson NH, Cowsert LM, Olson C, Brown JC. 1991. Structures of bovine and
880 human papillomaviruses. Analysis by cryoelectron microscopy and three-dimensional image
881 reconstruction. *Biophysical journal* **60**:1445–1456. doi: 10.1016/S0006-3495(91)82181-6.
882 **Ballut L**, Sapay N, Chautard E, Imberty A, Ricard-Blum S. 2013. Mapping of heparin/heparan sulfate
883 binding sites on αvβ3 integrin by molecular docking. *Journal of molecular recognition : JMR* **26**:76–
884 85. doi: 10.1002/jmr.2250.
885 **Becker M**, Greune L, Schmidt MA, Schelhaas M. 2018. Extracellular Conformational Changes in the
886 Capsid of Human Papillomaviruses Contribute to Asynchronous Uptake into Host Cells. *Journal of*
887 *virology* **92**. doi: 10.1128/jvi.02106-17.

888 **Bienkowska-Haba M**, Luszczek W, Myers JE, Keiffer TR, DiGiuseppe S, Polk P, Bodily JM, Scott RS,
889 Sapp M. 2018. A new cell culture model to genetically dissect the complete human papillomavirus
890 life cycle. *PLoS Pathogens* **14**:e1006846. doi: 10.1371/journal.ppat.1006846.
891 **Bienkowska-Haba M**, Patel HD, Sapp M. 2009. Target cell cyclophilins facilitate human
892 papillomavirus type 16 infection. *PLoS Pathogens* **5**:e1000524. doi: 10.1371/journal.ppat.1000524.
893 **Bruening J**, Lasswitz L, Banse P, Kahl S, Marinach C, Vondran FW, Kaderali L, Silvie O, Pietschmann T,
894 Meissner F, Gerold G. 2018. Hepatitis C virus enters liver cells using the CD81 receptor complex
895 proteins calpain-5 and CBLB. *PLoS Pathogens* **14**:e1007111. doi: 10.1371/journal.ppat.1007111.
896 **Buck CB**, Pastrana DV, Lowy DR, Schiller JT. 2004. Efficient intracellular assembly of papillomaviral
897 vectors. *Journal of virology* **78**:751–757. doi: 10.1128/jvi.78.2.751-757.2004.
898 **Bugatti A**, Zani A, Bardelli M, Giovanetti M, Ravelli C, Ciccozzi M, Caruso A, Caccuri F. 2025. Heparan
899 sulfate proteoglycans remodel SARS-CoV-2 spike conformation to allow integrin interaction and
900 infection of endothelial cells. *Frontiers in cellular and infection microbiology* **15**:1552116.
901 doi: 10.3389/fcimb.2025.1552116.
902 **Cagno V**, Tseligka ED, Jones ST, Tapparel C. 2019. Heparan Sulfate Proteoglycans and Viral
903 Attachment: True Receptors or Adaptation Bias? *Viruses* **11**. doi: 10.3390/v11070596.
904 **Cerqueira C**, Samperio Ventayol P, Vogeley C, Schelhaas M. 2015. Kallikrein-8 Proteolytically
905 Processes Human Papillomaviruses in the Extracellular Space To Facilitate Entry into Host Cells.
906 *Journal of virology* **89**:7038–7052. doi: 10.1128/JVI.00234-15.
907 **Chang K**, Baginski J, Hassan SF, Volin M, Shukla D, Tiwari V. 2016. Filopodia and Viruses: An Analysis
908 of Membrane Processes in Entry Mechanisms. *Frontiers in microbiology* **7**:300.
909 doi: 10.3389/fmicb.2016.00300.
910 **Christiansen IK**, Sandve GK, Schmitz M, Dürst M, Hovig E. 2015. Transcriptionally active regions are
911 the preferred targets for chromosomal HPV integration in cervical carcinogenesis. *PloS one*
912 **10**:e0119566. doi: 10.1371/journal.pone.0119566.
913 **Clausen TM**, Sandoval DR, Spliid CB, Pihl J, Perrett HR, Painter CD, Narayanan A, Majowicz SA, Kwong
914 EM, McVicar RN, Thacker BE, Glass CA, Yang Z, Torres JL, Golden GJ, Bartels PL, Porell RN,
915 Garretson AF, Laubach L, Feldman J, Yin X, Pu Y, Hauser BM, Caradonna TM, Kellman BP, Martino
916 C, Gordts PLSM, Chanda SK, Schmidt AG, Godula K, Leibel SL, Jose J, Corbett KD, Ward AB, Carlin
917 AF, Esko JD. 2020. SARS-CoV-2 Infection Depends on Cellular Heparan Sulfate and ACE2. *Cell*
918 **183**:1043-1057.e15. doi: 10.1016/j.cell.2020.09.033.
919 **Culp TD**, Budgeon LR, Marinkovich MP, Meneguzzi G, Christensen ND. 2006. Keratinocyte-secreted
920 laminin 5 can function as a transient receptor for human papillomaviruses by binding virions and
921 transferring them to adjacent cells. *Journal of virology* **80**:8940–8950. doi: 10.1128/JVI.00724-06.
922 **Dasgupta J**, Bienkowska-Haba M, Ortega ME, Patel HD, Bodevin S, Spillmann D, Bishop B, Sapp M,
923 Chen XS. 2011. Structural basis of oligosaccharide receptor recognition by human papillomavirus.
924 *The Journal of biological chemistry* **286**:2617–2624. doi: 10.1074/jbc.m110.160184.
925 **David G**, Bai XM, van der Schueren B, Cassiman JJ, van den Berghe H. 1992. Developmental changes
926 in heparan sulfate expression: in situ detection with mAbs. *The Journal of cell biology* **119**:961–
927 975. doi: 10.1083/jcb.119.4.961.
928 **Day PM**, Gambhira R, Roden RBS, Lowy DR, Schiller JT. 2008. Mechanisms of human papillomavirus
929 type 16 neutralization by l2 cross-neutralizing and l1 type-specific antibodies. *Journal of virology*
930 **82**:4638–4646. doi: 10.1128/JVI.00143-08.
931 **Day PM**, Schelhaas M. 2014. Concepts of papillomavirus entry into host cells. *Current opinion in*
932 *virology* **4**:24–31. doi: 10.1016/j.coviro.2013.11.002.
933 **Day PM**, Schiller JT. 2009. The role of furin in papillomavirus infection. *Future microbiology* **4**:1255–
934 1262. doi: 10.2217/fmb.09.86.

Doorbar J, Quint W, Banks L, Bravo IG, Stoler M, Broker TR, Stanley MA. 2012. The biology and life-cycle of human papillomaviruses. *Vaccine* **30 Suppl 5**:F55-70. doi: 10.1016/j.vaccine.2012.06.083.

Dziduszko A, Ozbun MA. 2013. Annexin A2 and S100A10 regulate human papillomavirus type 16 entry and intracellular trafficking in human keratinocytes. *Journal of virology* **87**:7502–7515. doi: 10.1128/JVI.00519-13.

Earnest JT, Hantak MP, Park J-E, Gallagher T. 2015. Coronavirus and influenza virus proteolytic priming takes place in tetraspanin-enriched membrane microdomains. *Journal of virology* **89**:6093–6104. doi: 10.1128/JVI.00543-15.

Evander M, Frazer IH, Payne E, Qi YM, Hengst K, McMillan NA. 1997. Identification of the alpha6 integrin as a candidate receptor for papillomaviruses. *Journal of virology* **71**:2449–2456. doi: 10.1128/JVI.71.3.2449-2456.1997.

Feng Y, van Bodegraven D, Kádek A, L B Munguira I, Soria-Martinez L, Nentwich S, Saha S, Chardon F, Kavan D, Uetrecht C, Schelhaas M, Roos WH. 2024. Glycan-induced structural activation softens the human papillomavirus capsid for entry through reduction of intercapsomere flexibility. *Nature communications* **15**:10076. doi: 10.1038/s41467-024-54373-0.

Finke J, Mikuličić S, Loster A-L, Gawlitza A, Florin L, Lang T. 2020. Anatomy of a viral entry platform differentially functionalized by integrins α3 and α6. *Scientific reports* **10**:5356. doi: 10.1038/s41598-020-62202-9.

Florin L, Lang T. 2018. Tetraspanin Assemblies in Virus Infection. *Frontiers in immunology* **9**:1140. doi: 10.3389/fimmu.2018.01140.

Galati L, Chiantore MV, Marinaro M, Di Bonito P. 2024a. Human Oncogenic Viruses: Characteristics and Prevention Strategies-Lessons Learned from Human Papillomaviruses. *Viruses* **16**. doi: 10.3390/v16030416.

Galati L, Di Bonito P, Marinaro M, Chiantore MV, Gheit T. 2024b. HPV16 Phylogenetic Variants in Anogenital and Head and Neck Cancers: State of the Art and Perspectives. *Viruses* **16**. doi: 10.3390/v16060904.

Gilson TD, Gibson RT, Androphy EJ. 2020. Optimization of human papillomavirus-based pseudovirus techniques for efficient gene transfer. *Scientific reports* **10**:15517. doi: 10.1038/s41598-020-72027-1.

Giroglou T, Florin L, Schäfer F, Streeck RE, Sapp M. 2001. Human papillomavirus infection requires cell surface heparan sulfate. *Journal of virology* **75**:1565–1570. doi: 10.1128/JVI.75.3.1565-1570.2001.

Hantak MP, Qing E, Earnest JT, Gallagher T. 2019. Tetraspanins: Architects of Viral Entry and Exit Platforms. *Journal of virology* **93**. doi: 10.1128/JVI.01429-17.

Hemler ME. 2005. Tetraspanin functions and associated microdomains. *Nature reviews. Molecular cell biology* **6**:801–811. doi: 10.1038/nrm1736.

Heuser J. 2000. The production of 'cell cortices' for light and electron microscopy. *Traffic (Copenhagen, Denmark)* **1**:545–552. doi: 10.1034/j.1600-0854.2000.010704.x.

Hochdorfer D, Florin L, Sinzger C, Lieber D. 2016. Tetraspanin CD151 Promotes Initial Events in Human Cytomegalovirus Infection. *Journal of virology* **90**:6430–6442. doi: 10.1128/jvi.00145-16.

Homsi Y, Schloetel J-G, Scheffer KD, Schmidt TH, Destainville N, Florin L, Lang T. 2014. The extracellular δ-domain is essential for the formation of CD81 tetraspanin webs. *Biophysical journal* **107**:100–113. doi: 10.1016/j.bpj.2014.05.028.

Jamieson RR, Stasiak SE, Polio SR, Augspurg RD, McCormick CA, Ruberti JW, Parameswaran H. 2021. Stiffening of the extracellular matrix is a sufficient condition for airway hyperreactivity. *Journal of applied physiology (Bethesda, Md. : 1985)* **130**:1635–1645. doi: 10.1152/japplphysiol.00554.2020.

Joyce JG, Tung JS, Przysiecki CT, Cook JC, Lehman ED, Sands JA, Jansen KU, Keller PM. 1999. The L1 major capsid protein of human papillomavirus type 11 recombinant virus-like particles interacts

983 with heparin and cell-surface glycosaminoglycans on human keratinocytes. *The Journal of*
984 *biological chemistry* **274**:5810–5822. doi: 10.1074/jbc.274.9.5810.
985 **Kines RC**, Thompson CD, Lowy DR, Schiller JT, Day PM. 2009. The initial steps leading to
986 papillomavirus infection occur on the basement membrane prior to cell surface binding.
987 *Proceedings of the National Academy of Sciences of the United States of America* **106**:20458–
988 20463. doi: 10.1073/pnas.0908502106.
989 **Knappe M**, Bodevin S, Selinka H-C, Spillmann D, Streeck RE, Chen XS, Lindahl U, Sapp M. 2007.
990 Surface-exposed amino acid residues of HPV16 L1 protein mediating interaction with cell surface
991 heparan sulfate. *The Journal of biological chemistry* **282**:27913–27922.
992 doi: 10.1074/jbc.m705127200.
993 **Martel C** de, Plummer M, Vignat J, Franceschi S. 2017. Worldwide burden of cancer attributable to
994 HPV by site, country and HPV type. *International journal of cancer* **141**:664–670.
995 doi: 10.1002/ijc.30716.
996 **Mikuličić S**, Finke J, Boukhallouk F, Wüstenhagen E, Sons D, Homsi Y, Reiss K, Lang T, Florin L. 2019.
997 ADAM17-dependent signaling is required for oncogenic human papillomavirus entry platform
998 assembly. *eLife* **8**. doi: 10.7554/eLife.44345.
999 **Mikuličić S**, Massenberg A, Döring T, Brandenburg K, Lang T, Florin L. 2025. HSPG-binding peptide
1000 Pep19-2.5 is a potent inhibitor of HPV16 infection. *Antimicrobial agents and chemotherapy*
1001 **69**:e0157524. doi: 10.1128/aac.01575-24.
1002 **Mikuličić S**, Strunk J, Florin L. 2021. HPV16 Entry into Epithelial Cells: Running a Gauntlet. *Viruses* **13**.
1003 doi: 10.3390/v13122460.
1004 **Miladinova E**, Lilkova E, Krachmarova E, Malinova K, Petkov P, Ilieva N, Nacheva G, Litov L. 2022.
1005 Heparan Sulfate Facilitates Binding of hIFNγ to Its Cell-Surface Receptor hIFNGR1. *International*
1006 *journal of molecular sciences* **23**. doi: 10.3390/ijms23169415.
1007 **Ozbun MA**. 2019. Extracellular events impacting human papillomavirus infections: Epithelial
1008 wounding to cell signaling involved in virus entry. *Papillomavirus research (Amsterdam,*
1009 *Netherlands)* **7**:188–192. doi: 10.1016/j.pvr.2019.04.009.
1010 **Ozbun MA**, Campos SK. 2021. The long and winding road: human papillomavirus entry and
1011 subcellular trafficking. *Current opinion in virology* **50**:76–86. doi: 10.1016/j.coviro.2021.07.010.
1012 **Pellegrini L**. 2001. Role of heparan sulfate in fibroblast growth factor signalling: a structural view.
1013 *Current opinion in structural biology* **11**:629–634. doi: 10.1016/s0959-440x(00)00258-x.
1014 **Peng GE**, Wilson SR, Weiner OD. 2011. A pharmacological cocktail for arresting actin dynamics in
1015 living cells. *Molecular biology of the cell* **22**:3986–3994. doi: 10.1091/mbc.E11-04-0379.
1016 **Richards KF**, Bienkowska-Haba M, Dasgupta J, Chen XS, Sapp M. 2013. Multiple heparan sulfate
1017 binding site engagements are required for the infectious entry of human papillomavirus type 16.
1018 *Journal of virology* **87**:11426–11437. doi: 10.1128/jvi.01721-13.
1019 **Richards KF**, Mukherjee S, Bienkowska-Haba M, Pang J, Sapp M. 2014. Human papillomavirus
1020 species-specific interaction with the basement membrane-resident non-heparan sulfate receptor.
1021 *Viruses* **6**:4856–4879. doi: 10.3390/v6124856.
1022 **Richards RM**, Lowy DR, Schiller JT, Day PM. 2006. Cleavage of the papillomavirus minor capsid
1023 protein, L2, at a furin consensus site is necessary for infection. *Proceedings of the National*
1024 *Academy of Sciences of the United States of America* **103**:1522–1527.
1025 doi: 10.1073/pnas.0508815103.
1026 **Rommel O**, Dillner J, Fligge C, Bergsdorf C, Wang X, Selinka H-C, Sapp M. 2005. Heparan sulfate
1027 proteoglycans interact exclusively with conformationally intact HPV L1 assemblies: basis for a
1028 virus-like particle ELISA. *Journal of medical virology* **75**:114–121. doi: 10.1002/jmv.20245.
1029 **Schaks M**, Giannone G, Rottner K. 2019. Actin dynamics in cell migration. *Essays in biochemistry*
1030 **63**:483–495. doi: 10.1042/EBC20190015.

1031 **Scheffer KD**, Gawlitza A, Spoden GA, Zhang XA, Lambert C, Berditchevski F, Florin L. 2013.
1032 Tetraspanin CD151 mediates papillomavirus type 16 endocytosis. *Journal of virology* **87**:3435–
1033 3446. doi: 10.1128/JVI.02906-12.
1034 **Schelhaas M**, Ewers H, Rajamäki M-L, Day PM, Schiller JT, Helenius A. 2008. Human papillomavirus
1035 type 16 entry: retrograde cell surface transport along actin-rich protrusions. *PLoS Pathogens*
1036 **4**:e1000148. doi: 10.1371/journal.ppat.1000148.
1037 **Schelhaas M**, Shah B, Holzer M, Blattmann P, Kühling L, Day PM, Schiller JT, Helenius A. 2012. Entry
1038 of human papillomavirus type 16 by actin-dependent, clathrin- and lipid raft-independent
1039 endocytosis. *PLoS Pathogens* **8**:e1002657. doi: 10.1371/journal.ppat.1002657.
1040 **Schiller JT**, Day PM, Kines RC. 2010. Current understanding of the mechanism of HPV infection.
1041 *Gynecologic oncology* **118**:S12-7. doi: 10.1016/j.ygyno.2010.04.004.
1042 **Schindelin J**, Arganda-Carreras I, Frise E, Kaynig V, Longair M, Pietzsch T, Preibisch S, Rueden C,
1043 Saalfeld S, Schmid B, Tinevez J-Y, White DJ, Hartenstein V, Eliceiri K, Tomancak P, Cardona A. 2012.
1044 Fiji: an open-source platform for biological-image analysis. *Nature methods* **9**:676–682.
1045 doi: 10.1038/nmeth.2019.
1046 **Schmidt SC**, Massenberg A, Homsi Y, Sons D, Lang T. 2024. Microscopic clusters feature the
1047 composition of biochemical tetraspanin-assemblies and constitute building-blocks of tetraspanin
1048 enriched domains. *Scientific reports* **14**:2093. doi: 10.1038/s41598-024-52615-1.
1049 **Selinka H-C**, Florin L, Patel HD, Freitag K, Schmidtke M, Makarov VA, Sapp M. 2007. Inhibition of
1050 transfer to secondary receptors by heparan sulfate-binding drug or antibody induces
1051 noninfectious uptake of human papillomavirus. *Journal of virology* **81**:10970–10980.
1052 doi: 10.1128/jvi.00998-07.
1053 **Selinka H-C**, Giroglou T, Sapp M. 2002. Analysis of the infectious entry pathway of human
1054 papillomavirus type 33 pseudovirions. *Virology* **299**:279–287. doi: 10.1006/viro.2001.1493.
1055 **Smith JL**, Lidke DS, Ozbun MA. 2008. Virus activated filopodia promote human papillomavirus type
1056 31 uptake from the extracellular matrix. *Virology* **381**:16–21. doi: 10.1016/j.virol.2008.08.040.
1057 **Spoden G**, Freitag K, Husmann M, Boller K, Sapp M, Lambert C, Florin L. 2008. Clathrin- and caveolin-
1058 independent entry of human papillomavirus type 16--involvement of tetraspanin-enriched
1059 microdomains (TEMs). *PloS one* **3**:e3313. doi: 10.1371/journal.pone.0003313.
1060 **Spoden G**, Kühling L, Cordes N, Frenzel B, Sapp M, Boller K, Florin L, Schelhaas M. 2013. Human
1061 papillomavirus types 16, 18, and 31 share similar endocytic requirements for entry. *Journal of*
1062 *virology* **87**:7765–7773. doi: 10.1128/jvi.00370-13.
1063 **Spoden GA**, Besold K, Krauter S, Plachter B, Hanik N, Kilbinger AFM, Lambert C, Florin L. 2012.
1064 Polyethylenimine is a strong inhibitor of human papillomavirus and cytomegalovirus infection.
1065 *Antimicrobial agents and chemotherapy* **56**:75–82. doi: 10.1128/aac.05147-11.
1066 **Surviladze Z**, Dziduszko A, Ozbun MA. 2012. Essential Roles for Soluble Virion-Associated Heparan
1067 Sulfonated Proteoglycans and Growth Factors in Human Papillomavirus Infections. *PLoS*
1068 *Pathogens* **8**:e1002519. doi: 10.1371/journal.ppat.1002519.
1069 **Surviladze Z**, Sterkand RT, Ozbun MA. 2015. Interaction of human papillomavirus type 16 particles
1070 with heparan sulfate and syndecan-1 molecules in the keratinocyte extracellular matrix plays an
1071 active role in infection. *The Journal of general virology* **96**:2232–2241. doi: 10.1099/vir.0.000147.
1072 **Tian J**, Li C, Li W. 2021. Entry of hepatitis B virus: going beyond NTCP to the nucleus. *Current opinion*
1073 *in virology* **50**:97–102. doi: 10.1016/j.coviro.2021.08.001.
1074 **Vasioukhin V**, Bauer C, Yin M, Fuchs E. 2000. Directed actin polymerization is the driving force for
1075 epithelial cell-cell adhesion. *Cell* **100**:209–219. doi: 10.1016/s0092-8674(00)81559-7.
1076 **Woodham AW**, Da Silva DM, Skeate JG, Raff AB, Ambroso MR, Brand HE, Isas JM, Langen R, Kast
1077 WM. 2012. The S100A10 subunit of the annexin A2 heterotetramer facilitates L2-mediated human
1078 papillomavirus infection. *PloS one* **7**:e43519. doi: 10.1371/journal.pone.0043519.

1079 **Wüstenhagen E**, Boukhallouk F, Negwer I, Rajalingam K, Stubenrauch F, Florin L. 2018. The Myb-
1080 related protein MYPOP is a novel intrinsic host restriction factor of oncogenic human
1081 papillomaviruses. *Oncogene* **37**:6275–6284. doi: 10.1038/s41388-018-0398-6.
1082 **Yokoyama H**, Sato K, Okudaira M, Morita C, Takahashi C, Suzuki D, Sakai H, Iwamoto Y. 1999. Serum
1083 and urinary concentrations of heparan sulfate in patients with diabetic nephropathy. *Kidney*
1084 *international* **56**:650–658. doi: 10.1046/j.1523-1755.1999.00591.x.
1085 **Yoon CS**, Kim KD, Park SN, Cheong SW. 2001. alpha(6) Integrin is the main receptor of human
1086 papillomavirus type 16 VLP. *Biochemical and biophysical research communications* **283**:668–673.
1087 doi: 10.1006/bbrc.2001.4838.
1088 **Zhang Q**, Tang W, Stancanelli E, Jung E, Syed Z, Pagadala V, Saidi L, Chen CZ, Gao P, Xu M, Pavlinov I,
1089 Li B, Huang W, Chen L, Liu J, Xie H, Zheng W, Ye Y. 2023. Host heparan sulfate promotes ACE2
1090 super-cluster assembly and enhances SARS-CoV-2-associated syncytium formation. *Nature*
1091 *communications* **14**:5777. doi: 10.1038/s41467-023-41453-w.
1092 **Zona L**, Lupberger J, Sidahmed-Adrar N, Thumann C, Harris HJ, Barnes A, Florentin J, Tawar RG, Xiao
1093 F, Turek M, Durand SC, Duong FHT, Heim MH, Cosset F-L, Hirsch I, Samuel D, Brino L, Zeisel MB, Le
1094 Naour F, McKeating JA, Baumert TF. 2013. HRas signal transduction promotes hepatitis C virus cell
1095 entry by triggering assembly of the host tetraspanin receptor complex. *Cell host & microbe*
1096 **13**:302–313. doi: 10.1016/j.chom.2013.02.006.
1097 **zur Hausen H**. 2009. The search for infectious causes of human cancers: where and why (Nobel
1098 lecture). *Angewandte Chemie (International ed. in English)* **48**:5798–5808.
1099 doi: 10.1002/anie.200901917.
1100

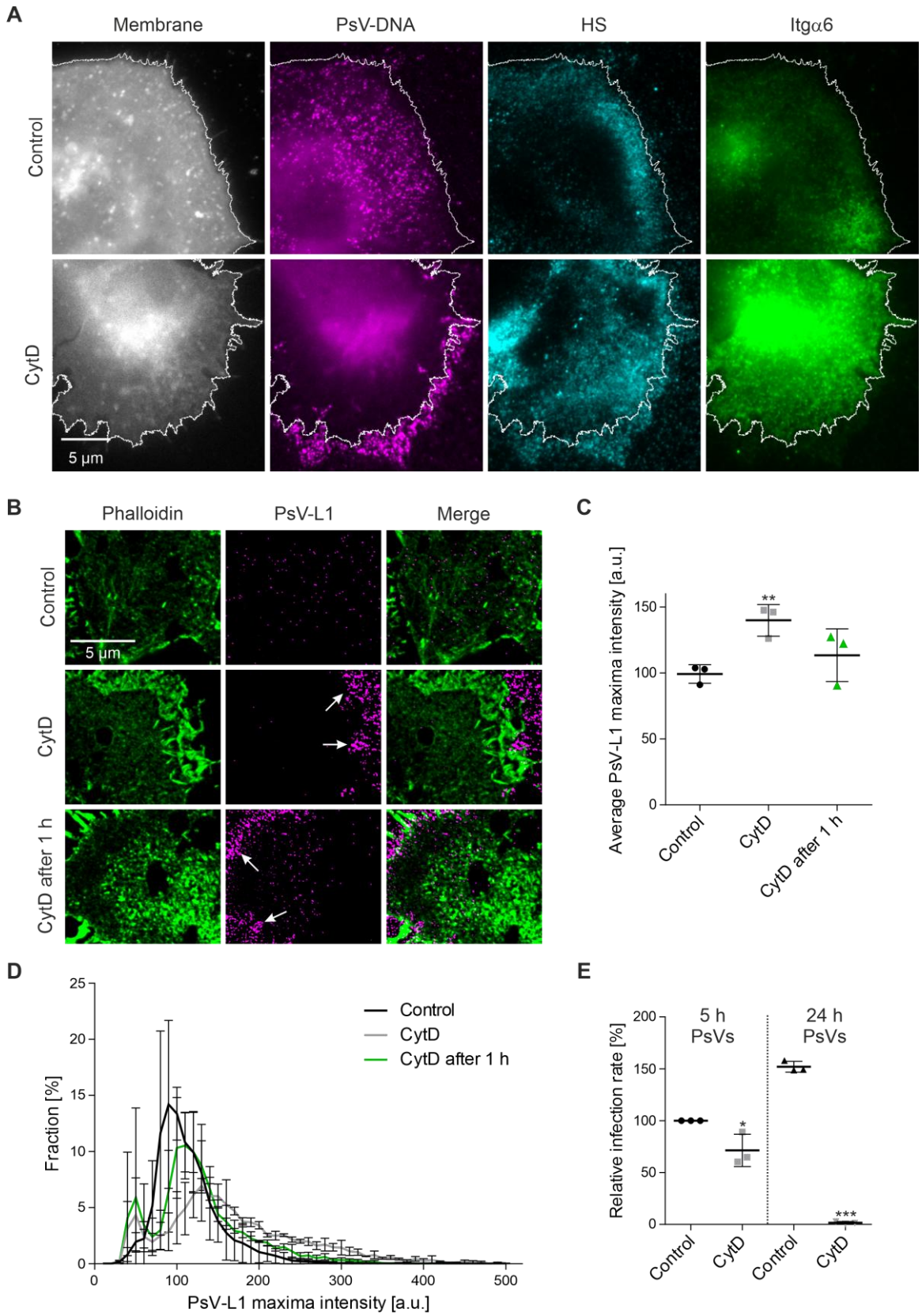

Figure 1. *CytD arrests PsV recruitment from the ECM to the cell body.*
(A) In the absence (Control) or presence of 10 µg/ml CytD (CytD), HaCaT cells were incubated with PsVs at 37 °C for 5 h. Then, cells were fixed, washed and stained with the cell membrane dye TMA-DPH (gray lookup table (LUT)). PsVs (magenta LUT) were visualized through coupling a dye (6-FAM Azide) to the encapsidated plasmid by click-chemistry. Indirect immunolabeling was employed for

1107 staining of HS (AlexaFluor 594; cyan LUT) and Itgα6 (STARRED; green LUT). Imaging was realized with
1108 epi-fluorescence microscopy. White lines delineate the main cell body; lines were created with
1109 reference to the TMA-DPH membrane staining. (B) Same pre-treatment of cells as in (A), with an
1110 additional condition where CytD was added 1 h after the PsVs (CytD after 1 h). Prior to fixation,
1111 membrane sheets were generated and F-actin was stained with phalloidin coupled to iFluor488 (green
1112 LUT). The capsid protein L1 of the PsVs and CD151 were stained by immunofluorescence using primary
1113 antibodies in combination with AlexaFluor 594-labelled (L1, magenta LUT) and STAR RED-labelled
1114 (CD151, not shown in this figure for clarity reasons) secondary antibodies. Images of phalloidin and L1
1115 staining were acquired in the confocal and STED mode of a STED microscope, respectively. Arrows in
1116 the PsV-L1 images point towards accumulated PsVs that after CytD are more frequently observed than
1117 in the control (see text). (C) Analysis of images as shown in (B) using ROIs covering the whole image.
1118 PsV maxima were detected and their intensities were quantified in a circular 125 nm diameter region
1119 of interest (ROI), followed by background correction. Values are given as means ± SD (n = 3; one
1120 biological replicate includes per condition the average of 14 - 15 analyzed membranes (intensity values
1121 of one membrane sheet were averaged) with altogether at least 1000 maxima intensity values). (D)
1122 PsV maxima intensity distribution of the data in (C). The fraction of PsVs, expressed in percent, is
1123 plotted as histogram (10 a.u. bins) against the maxima intensity. Values are given as means ± SD (n =
1124 3). (E) HaCaT cells were treated either for 5 h or 24 h with PsVs, without (Control) or with 10 µg/ml
1125 CytD (CytD). In case of the 5 h incubation, after removal of the PsVs/CytD cells were incubated for
1126 another 19 h in medium (in total 24 h). After a total of 24 h incubation, the luciferase activity of lysed
1127 cells was measured, yielding the infection rate that was normalized to LDH, resulting in the normalized
1128 infection rate. The normalized infection rate was further related to the mean normalized infection
1129 rate of the 5 h control, set to 100%, yielding the relative infection rate. Values are given as means ±
1130 SD (n = 3 biological replicates; the value of one biological replicate is the average of three technical
1131 replicates). (C) and (E). Statistical differences between Control and CytD was analyzed by using the
1132 two-tailed, unpaired student's *t*-test (n = 3, for details see methods). a.u., arbitrary units.

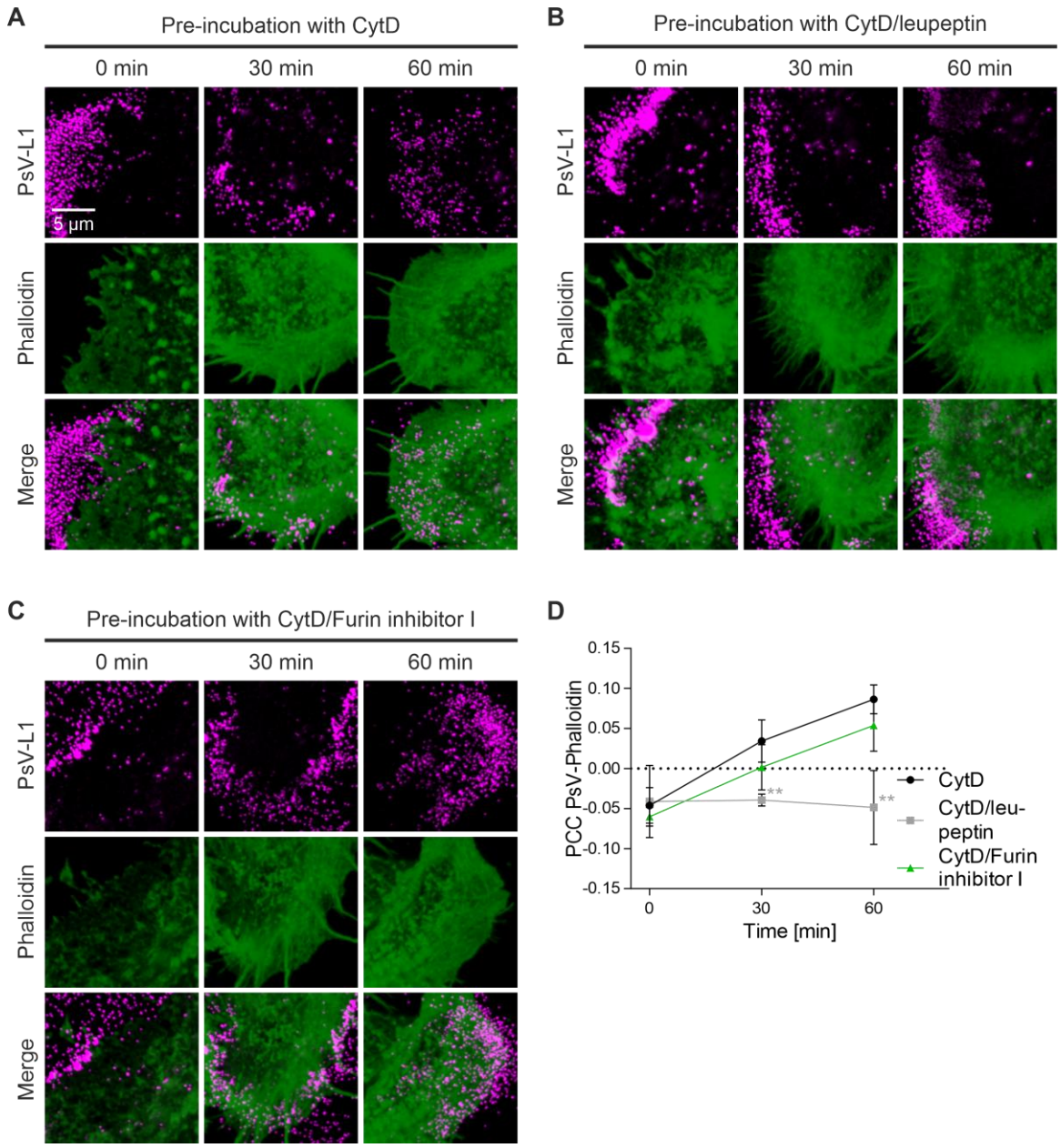

Figure 2. *Recruitment of PsVs from the ECM to the cell body requires PsV priming.* HaCaT cells were pre-incubated for 5 h at 37 °C with PsVs, in the presence of (A) 10 µg/ml CytD (CytD), (B) 10 µg/ml CytD and 100 µM leupeptin (CytD/leupeptin), or (C) 10 µg/ml CytD and 5 µM Furin inhibitor I (CytD/Furin inhibitor I). Afterwards, cells were washed and incubated without PsVs/inhibitors further for 0 min, 30 min or 60 min, before they were fixed and stained by indirect immunofluorescence for L1 (STAR GREEN, magenta LUT) and for F-actin by iFluor647-labelled phalloidin (green LUT). PsVs-L1 and F-actin staining were imaged in the confocal mode of a STED microscope. (D) For determination of the Pearson correlation coefficient (PCC) between PsV-L1 (magenta LUT) and Phalloidin (green LUT), we placed large ROIs onto the images that covered mainly the cell body but included parts of the cell periphery as well. The PCC was plotted over time. Values are given as means ± SD (n = 3 biological replicates). Statistical difference between CytD and CytD/inhibitors was analyzed by using the two-tailed, unpaired student's *t*-test (n = 3, for details see methods).

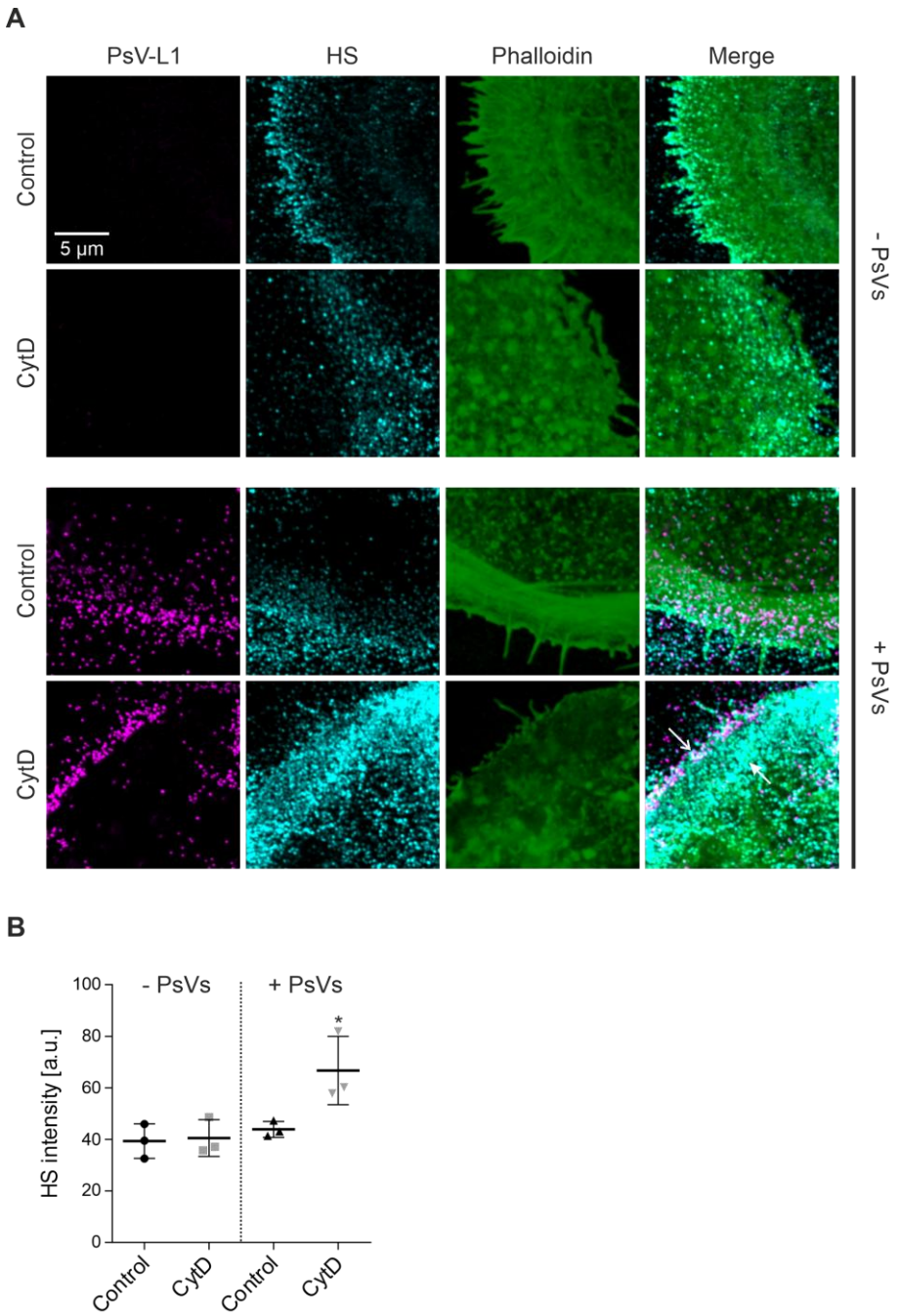

Figure 3. *Increased HS intensity after incubation with PsVs and CytD.*
(A) HaCaT cells were incubated without (top) and with (bottom) PsVs at 37 °C for 5 h, in the absence (Control, upper panels) or presence of 10 µg/ml CytD (CytD, lower panels). Afterwards, cells were washed, fixed and stained. Immunofluorescence was used for L1 (STAR GREEN; magenta LUT) and for HS (AlexaFluor 594; cyan LUT) staining. F-actin was stained by iFluor647-labelled phalloidin (green LUT). PsVs-L1, HS and F-actin staining were imaged in the confocal mode of a STED microscope. The open arrow marks a region where PsVs overlap with HS. The closed arrow marks a region devoid of PsVs showing strong HS staining. (B) For analysis of the mean HS intensity, we placed large ROIs onto the images covering mainly the cell body but including parts of the cell periphery as well. Values are given as means ± SD (n = 3 biological replicates). Statistical differences between Control and CytD were analyzed by using the two-tailed, unpaired student's *t*-test (n = 3, for details see methods).

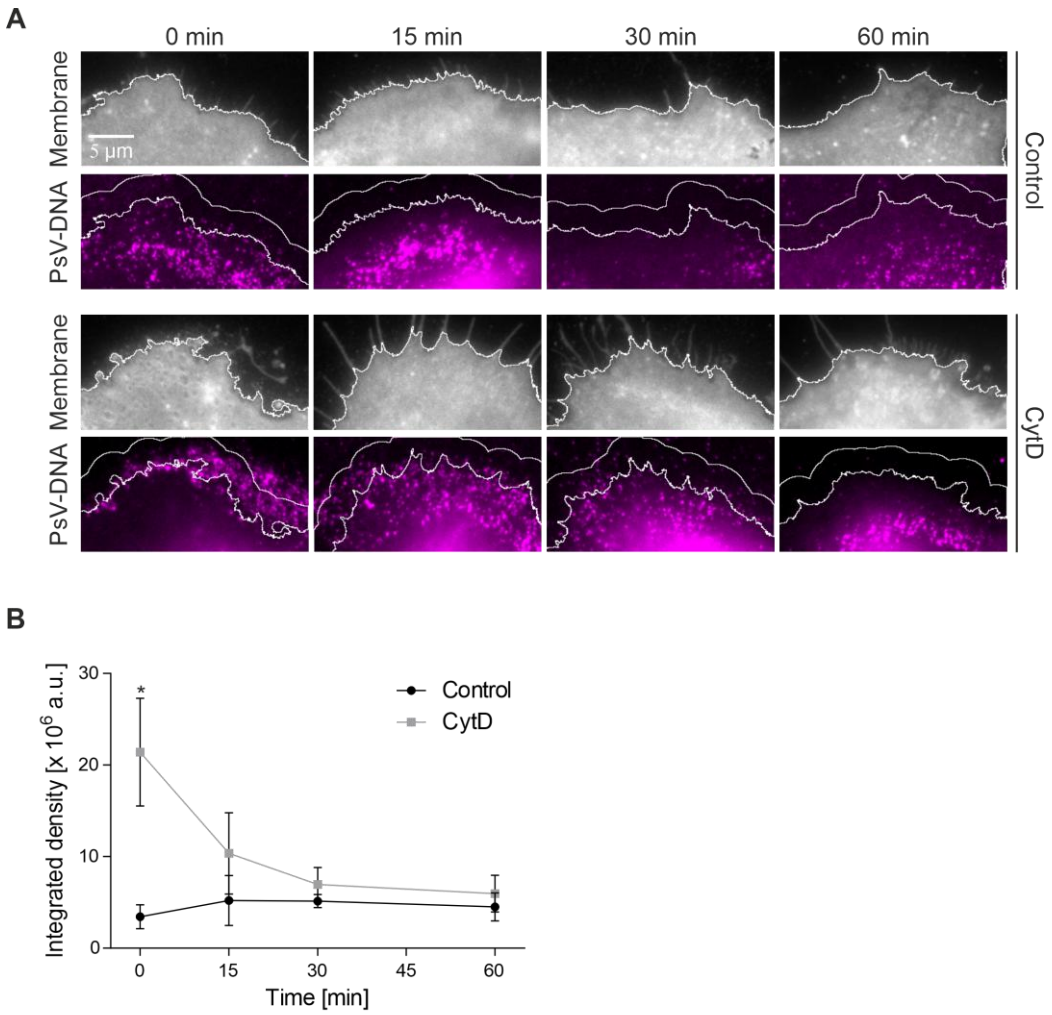

Figure 4. *Fast diminishment of accumulated PsVs at the cell periphery after removal of CytD.* (A) HaCaT cells were incubated with PsVs at 37 °C for 5 h, in the absence (Control) or presence of 10 µg/ml CytD (CytD). Then, cells were washed and incubated for the indicated time periods without PsVs/CytD, before they were fixed and stained as in Figure 1 (t = 0 min is identical to Figure 1A; for clarity we show only the membrane (gray LUT; images are shown at different settings of brightness and contrast) and the PsV-DNA staining (magenta LUT; images are shown at the same settings of brightness and contrast). The white lines in the membrane images delineate the cell body from the periphery. They were created with reference to the membrane staining (for details see methods). Using the cell body delineation as starting point, an up to 30-pixel broad area was created (PsV channel, magenta LUT; areas enclosed by the smoother white lines and the cell body delineation lines). The areas enclosed by the white lines define the cell peripheries. (B) The PsV-DNA signal of the periphery was quantified as integrated density, background corrected, and plotted over time. Values are given as means ± SD (n = 3 biological replicates). The statistical difference between the same time points of Control and CytD were analyzed by using the two-tailed, unpaired student's *t*-test (n = 3, for details see methods).

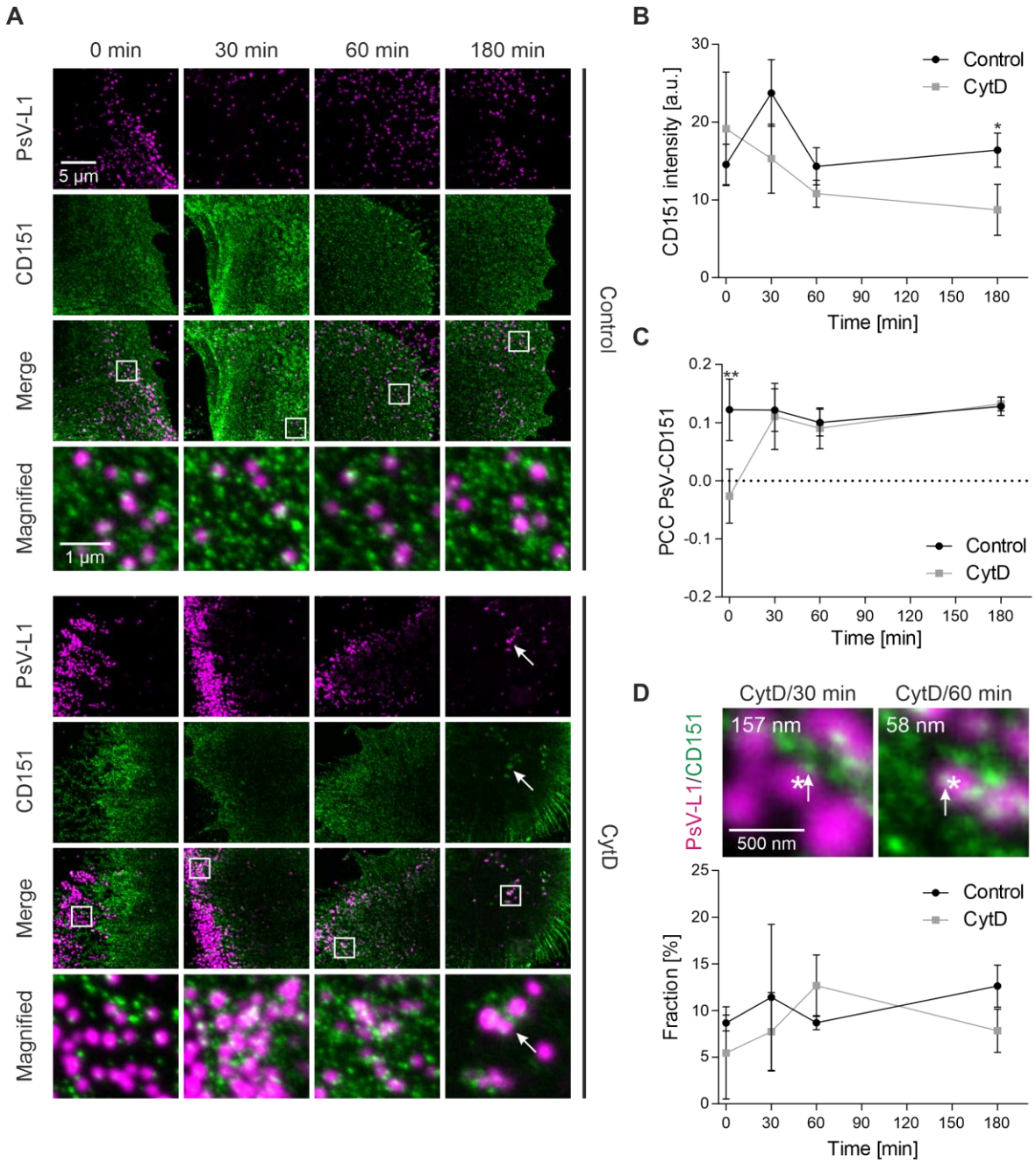

Figure 5. *Association between PsVs and CD151 occurs early in the infection cascade.*
(A) HaCaT cells were incubated with PsVs at 37 °C for 5 h, in the absence (Control, upper panels) or presence of 10 µg/ml CytD (CytD, lower panels). Afterwards, cells were washed and incubated without PsVs/CytD further for 0 min, 30 min, 60 min or 180 min, before they were fixed and stained by indirect immunofluorescence for L1 (STAR GREEN; magenta LUT) and for CD151 (AlexaFluor 594; green LUT), and for F-actin by iFluor647-labelled phalloidin (here not shown for clarity, please see Supplementary Figure 2A for F-actin staining illustrating the variability of filopodia after CytD treatment). The bottom rows show magnified views of the merged images from the regions marked by the white boxes. PsV-L1 and F-actin staining were imaged in the confocal and CD151 staining in the STED mode of a STED microscope, respectively. Therefore, compared to CD151, the PsVs are less resolved and also appear much larger than their real physical size (see magnified views). CytD/180 min, arrows mark presumably endocytic structures that formed in the central cell body region (for more examples see Supplementary Figure 4). For analysis, we placed large ROIs onto the images that covered mainly the

1190 cell body but included parts of the cell periphery as well (for an example ROI see Supplementary Figure
1191 5A). (B) The mean CD151 intensity was measured and plotted over time. (C) The PCC between PsV-L1
1192 (magenta LUT) and CD151 (green LUT) was calculated and plotted over time. (D) The fraction of PsVs
1193 (in percent) that have a distance to the next neighbored CD151 maximum ≤ 80 nm, which we define
1194 as closely associated, is plotted over time. Please note that the values in (D) were corrected for random
1195 background association (for details see Supplementary Figure 7). Two examples of PsVs (each marked
1196 by an asterisk) from the CytD/30 min (left) and CytD/60 min (right) conditions are shown. The value in
1197 the upper left states the shortest distance between the PsV and the next nearest CD151 maximum
1198 (marked by an arrow) in nm. Values are given as means ± SD (n = 3 biological replicates). Statistical
1199 differences between the same time points of Control and CytD were analyzed by using the two-tailed,
1200 unpaired student's *t*-test (n = 3, for details see methods).

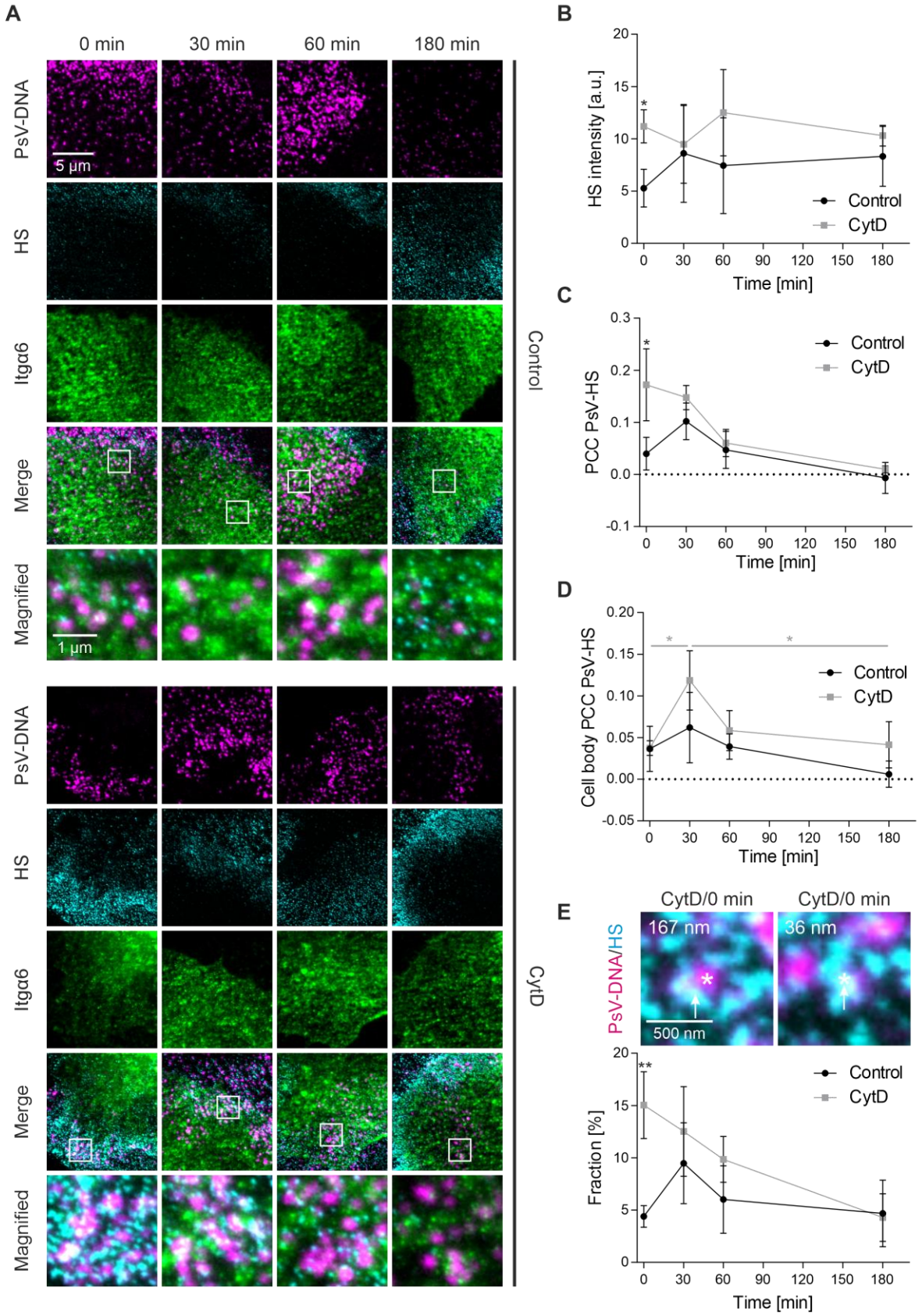

Figure 6. *Association between PsVs and HS after CytD treatment.*
(A) HaCaT cells were incubated with PsVs at 37 °C for 5 h, in the absence (Control, upper panels) or presence of 10 µg/ml CytD (CytD, lower panels). Afterwards, cells were washed and incubated without

1205 PsVs/CytD further for up to 180 min, before they were fixed and stained. PsVs (magenta LUT) were
1206 visualized by click-chemistry (6-FAM Azide) and indirect immunolabeling was used for HS (AlexaFluor
1207 594; cyan LUT) and for Itgα6 (STAR RED; green LUT). The bottom rows show magnified views of the
1208 white boxes in the merged images. PsV-DNA staining was imaged in the confocal and HS and Itgα6
1209 staining in the STED mode of a STED microscope. For analysis, we placed large ROIs onto the images
1210 that covered mainly the cell body but included parts of the cell periphery as well (see example in
1211 Supplementary Figure 8A). For (D), smaller ROIs covering only the cell body region were used. (B) The
1212 mean HS intensity plotted over time. (C) The PCC between PsV-DNA (magenta LUT) and HS (cyan LUT)
1213 over time. (D) The PCC between PsV-DNA (magenta LUT) and HS (cyan LUT) in the region of the cell
1214 body over time. (E) The fraction of PsVs (in percent) closely associating with HS (distance ≤ 80 nm)
1215 plotted over time (for background correction see Supplementary Figure 9). Two examples of PsVs
1216 (each marked by an asterisk) from the CytD/0 min condition are shown. The value in the upper left
1217 corner states the shortest distance (in nm) between the marked PsV and its next nearest HS maximum
1218 (marked by an arrow). Values are given as means ± SD (n = 3 biological replicates). Using the two-
1219 tailed, unpaired student's *t*-test (n = 3 biological replicates), we analyzed in (B), (C) and (E) the
1220 statistical differences between the same time points of Control and CytD, and in (D) the difference
1221 between CytD/30 min and CytD/0 min or CytD/180 min (for details see methods).
1222

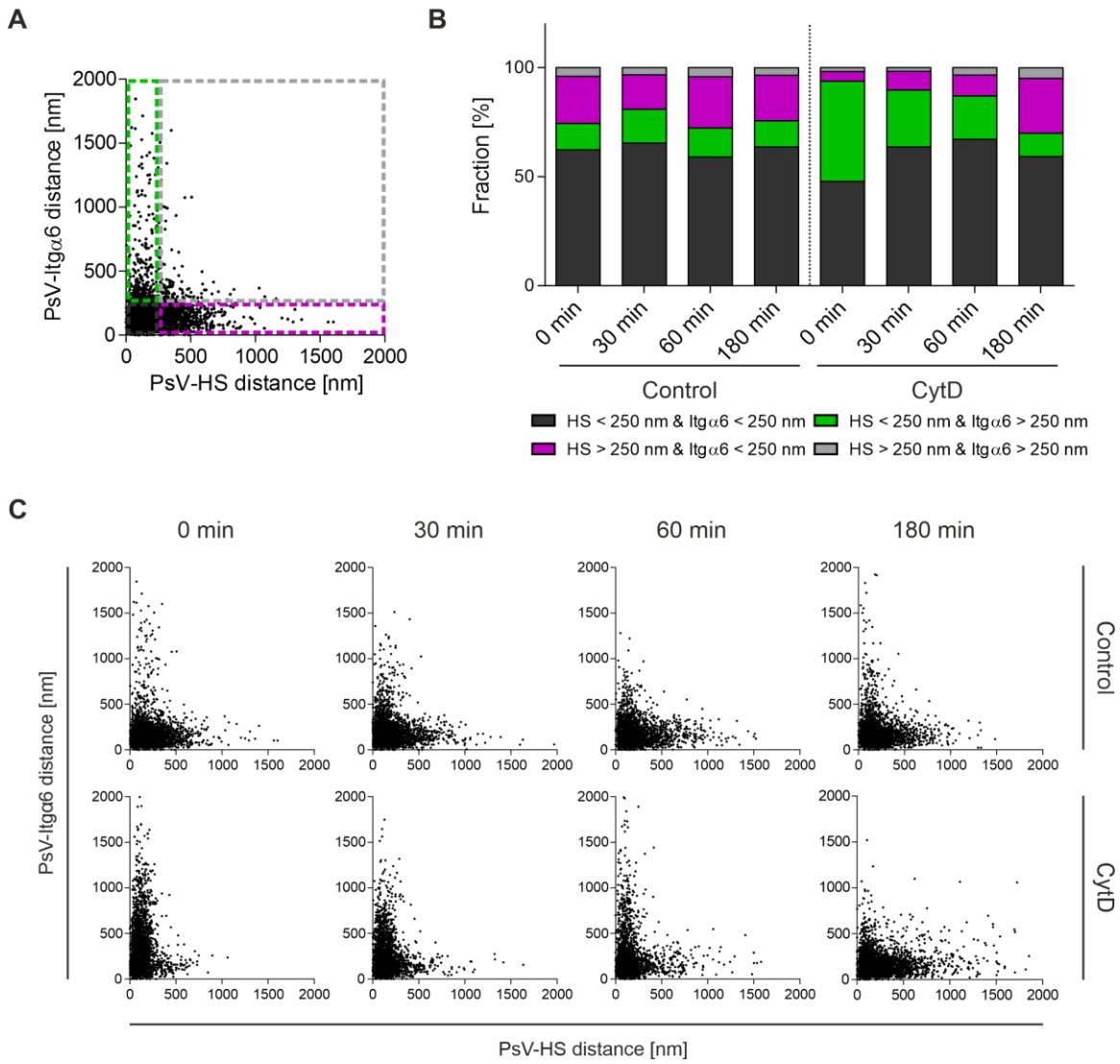

Figure 7. *PsV-Itgα6 and PsV-HS distances over time.*
(A) Definition of four PsV populations based on the PsV distances to Itgα6 and HS (please note that the data does not include distances of exactly 250 nm wherefore symbols as ≥ and ≤ are omitted; the plot is taken from Control, 0 min and shown again in C). Dashed green rectangle, PsVs with a distance to HS < 250 nm and to Itgα6 > 250 nm. Dashed magenta rectangle, PsVs with a distance to HS > 250 nm and to Itgα6 < 250 nm. Dashed gray square, PsVs with a distance to HS > 250 nm and to Itgα6 > 250 nm. PsVs not included in the previous categories have a distance to HS < 250 nm and to Itgα6 < 250 nm (dashed black square). (B) From the PsVs analyzed in Figure 6, for the Control (left) and CytD (right) the PsV fraction size (in percent) of each population is illustrated. Shown are the means of three biological replicates. For means ± SD and statistical analysis see Supplementary Table 1. (C) For the Control (top) and CytD (bottom), for each PsV, we plotted the shortest distance to Itgα6 against the shortest distance to HS (pooling the three biological replicates; 3,043 – 4,080 PsVs per plot).

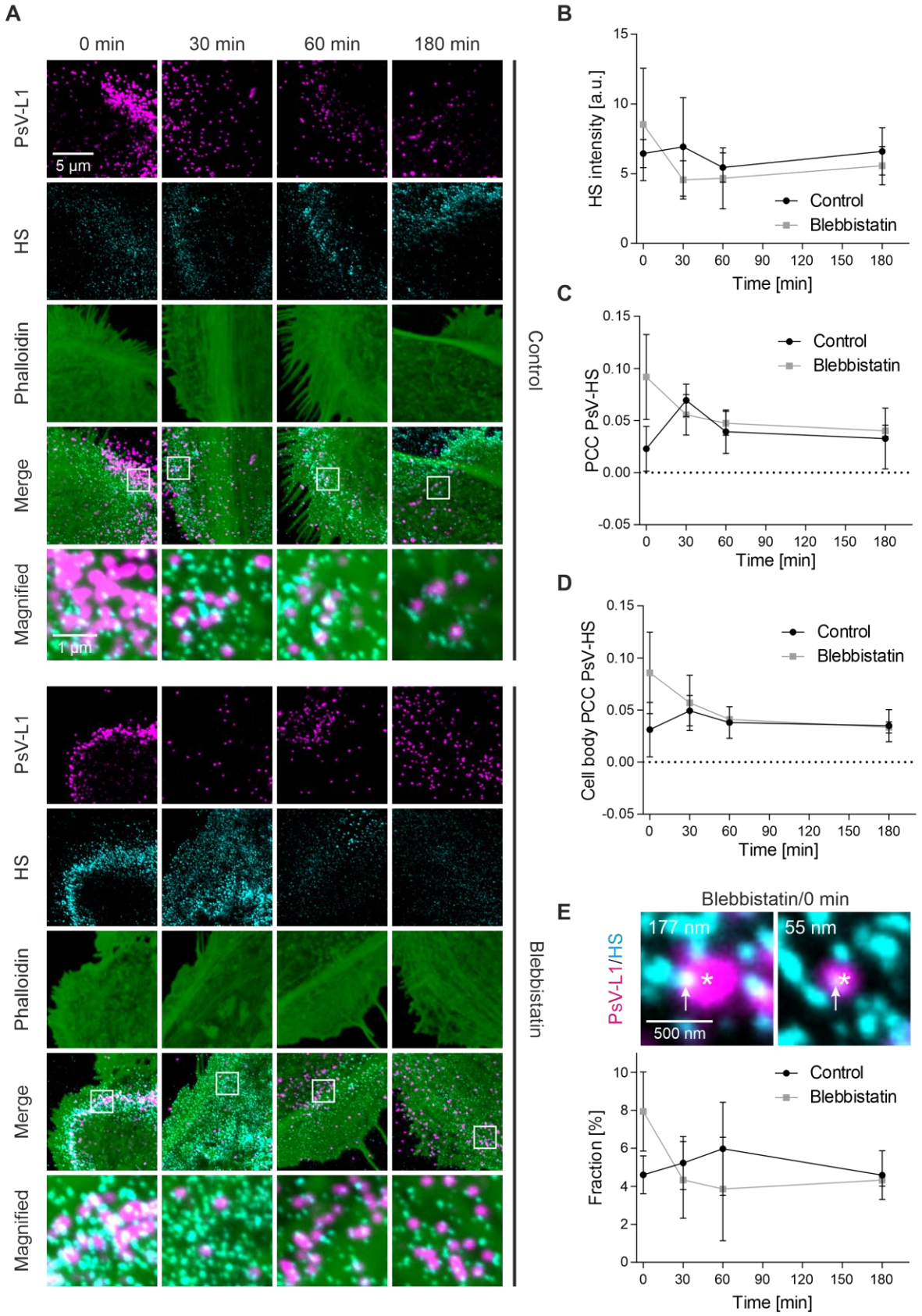

Figure 8. *Association between PsVs and HS after blebbistatin treatment.*
(A) HaCaT cells were incubated with PsVs at 37 °C for 5 h, in the absence (Control, upper panels) or presence of 30 µM blebbistatin (Blebbistatin, lower panels). Afterwards, cells were washed and

1241 incubated without PsVs/blebbistatin further for up to 180 min, before they were fixed and stained.
1242 Immunofluorescence was used for L1 (STAR GREEN; magenta LUT) and HS (AlexaFluor 594; cyan LUT)
1243 staining. F-actin was stained by iFluor647-labelled phalloidin (green LUT). The bottom rows show
1244 magnified views of the white boxes in the merged images. PsVs and F-actin staining were imaged in
1245 the confocal and HS staining in the STED mode of a STED microscope. For analysis, we placed large
1246 ROIs onto the images that covered mainly the cell body but included parts of the cell periphery as well.
1247 For (D), smaller ROIs covering only the cell body region were used. (B) Mean HS intensity over time.
1248 (C) PCC between PsV-L1 (magenta LUT) and HS (cyan LUT) over time (for control with flipped images
1249 see Supplementary Figure 10A and B). (D) PCC between PsV-L1 (magenta LUT) and HS (cyan LUT) in
1250 the region of the cell body over time (for control with flipped images see Supplementary Figure 10C
1251 and D). (E) The fraction of PsVs (in percent) closely associating with HS (distance ≤ 80 nm) plotted over
1252 time (for background correction see Supplementary Figure 11). Two examples of PsVs (each marked
1253 by an asterisk) from the blebbistatin/0 min condition are shown. The value in the upper left states the
1254 shortest distance between the PsV and its next nearest HS maximum (marked by an arrow) in nm.
1255 Values are given as means ± SD (n = 3 biological replicates). Statistical differences between the same
1256 time points of Control and Blebbistatin were analyzed by using the two-tailed, unpaired student's *t*-
1257 test (n = 3), but the analysis yielded no p-values below 0.05.
1258

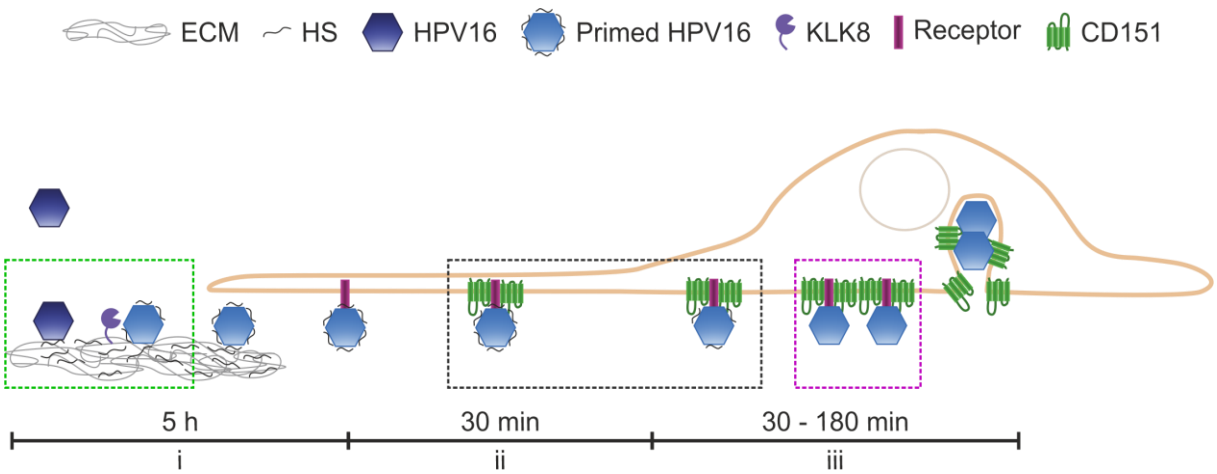

Figure 9. *Model of ECM events, recruitment, and receptor engagement in HPV16 entry.* (i) During 5 h of incubation with CytD, the PsVs bind to HS of the ECM, are primed, and become coated with HS cleavage products, enabling them for cell surface receptor engagement. After CytD removal, within 15 min, HS-decorated viruses are actively recruited to the cell body and (ii) associate with CD151 assemblies (completed within 30 min). (iii) Eventually, they lose their HS coat, and individual HPV16-CD151 assemblies agglomerate into larger structures (platforms), which are subsequently endocytosed. Dashed rectangles mark PsVs belonging to populations as defined in Figure 7. Dashed green rectangle, PsVs with a distance to HS < 250 nm and to Itgα6 > 250 nm. Dashed black rectangle, PsVs with a distance to HS < 250 nm and to Itgα6 < 250 nm. Dashed magenta rectangle, PsVs with a distance to HS > 250 nm and to Itgα6 < 250 nm.

1270 **Supplementary information**

1271

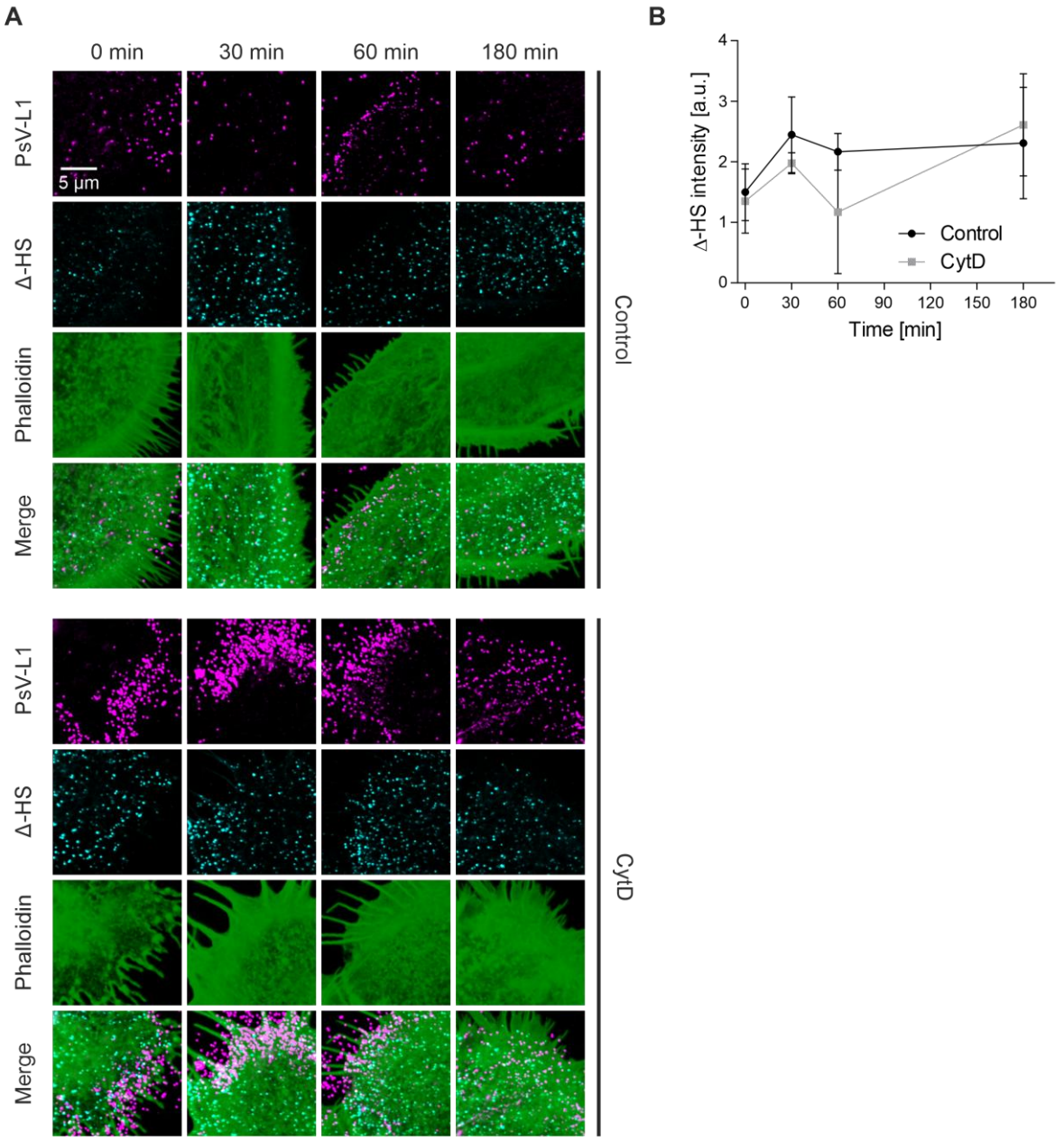

1272
1273

1274 **Supplementary Figure 1.** *HS neo-epitope (Δ-HS) staining after CytD treatment.*
1275 (A) HaCaT cells were incubated with PsVs at 37 °C for 5 h, in the absence (Control, upper panels) or
1276 presence of 10 µg/ml CytD (CytD, lower panels). Afterwards, cells were washed and incubated without
1277 PsVs/CytD further for up to 180 min, before they were fixed and stained. Immunofluorescence was
1278 used for the visualization of L1 (STAR GREEN; magenta LUT) and the HS neo-epitope, referred to as Δ-
1279 HS (AlexaFluor 594; cyan LUT). F-actin was stained by iFluor647-labelled phalloidin (green LUT). PsV-
1280 L1, Δ-HS and F-actin staining were imaged in the confocal mode of a STED microscope. For analysis,
1281 we placed large ROIs onto the images that covered mainly the cell body but included parts of the cell
1282 periphery as well. (B) The mean Δ-HS intensity over time. Values are given as means ± SD (n = 3
1283 biological replicates). Statistical differences between the same time points of Control and CytD were
1284 analyzed by using the two-tailed, unpaired student's *t*-test (n = 3), but the analysis yielded no p-values
1285 below 0.05.

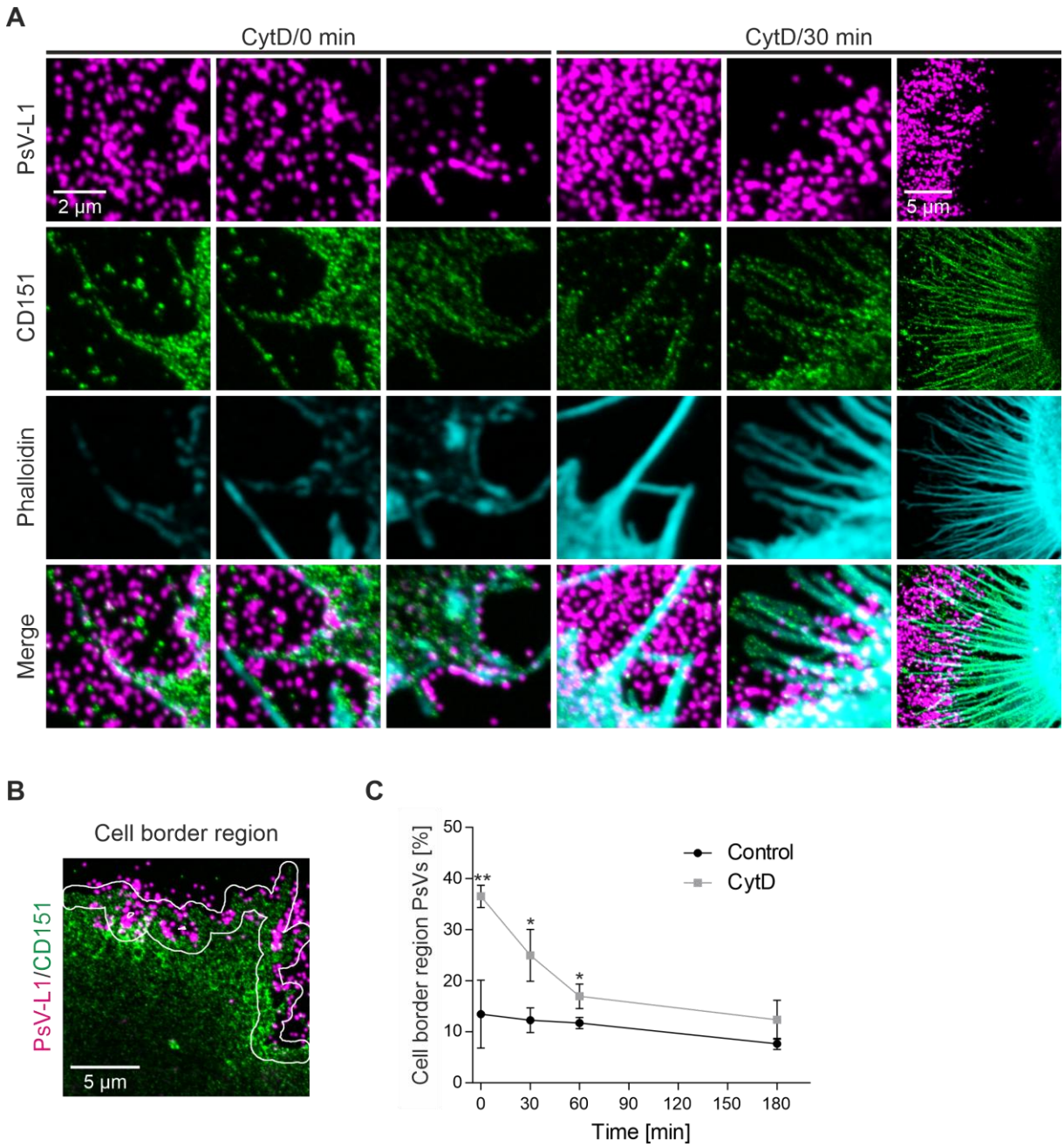

Supplementary Figure 2. *Variability of filopodia/diminishment of PsVs from the cell border region after CytD removal.*

(A) More images from the experiment described in Figure 5. We observed that many cells exhibit filopodia. Due to the large variability in number and shape we cannot show a representative image. Instead, we present for the CytD condition (0 min and 30 min) a variety of cells with CD151 positive filopodia. (B) Based on the CD151 image (green LUT), a cell border strip is defined and broadened by 20 pixels on each side, in the following referred to as the cell border region (for details see materials and methods). Please note that the cell border region is different from the cell periphery described in Figure 4 that delineates the cell body from the periphery. Instead, the cell border region covers both cell body and periphery (approximately two thirds inside and one third outside of the cell; for details see methods). (C) PsV maxima in the cell border region over time, expressed as percentage of all PsVs present in the image. Values are given as means ± SD (n = 3 biological replicates). Statistical differences between the same time points of Control and CytD were analyzed by using the two-tailed, unpaired student's *t*-test (n = 3, for details see materials and methods).

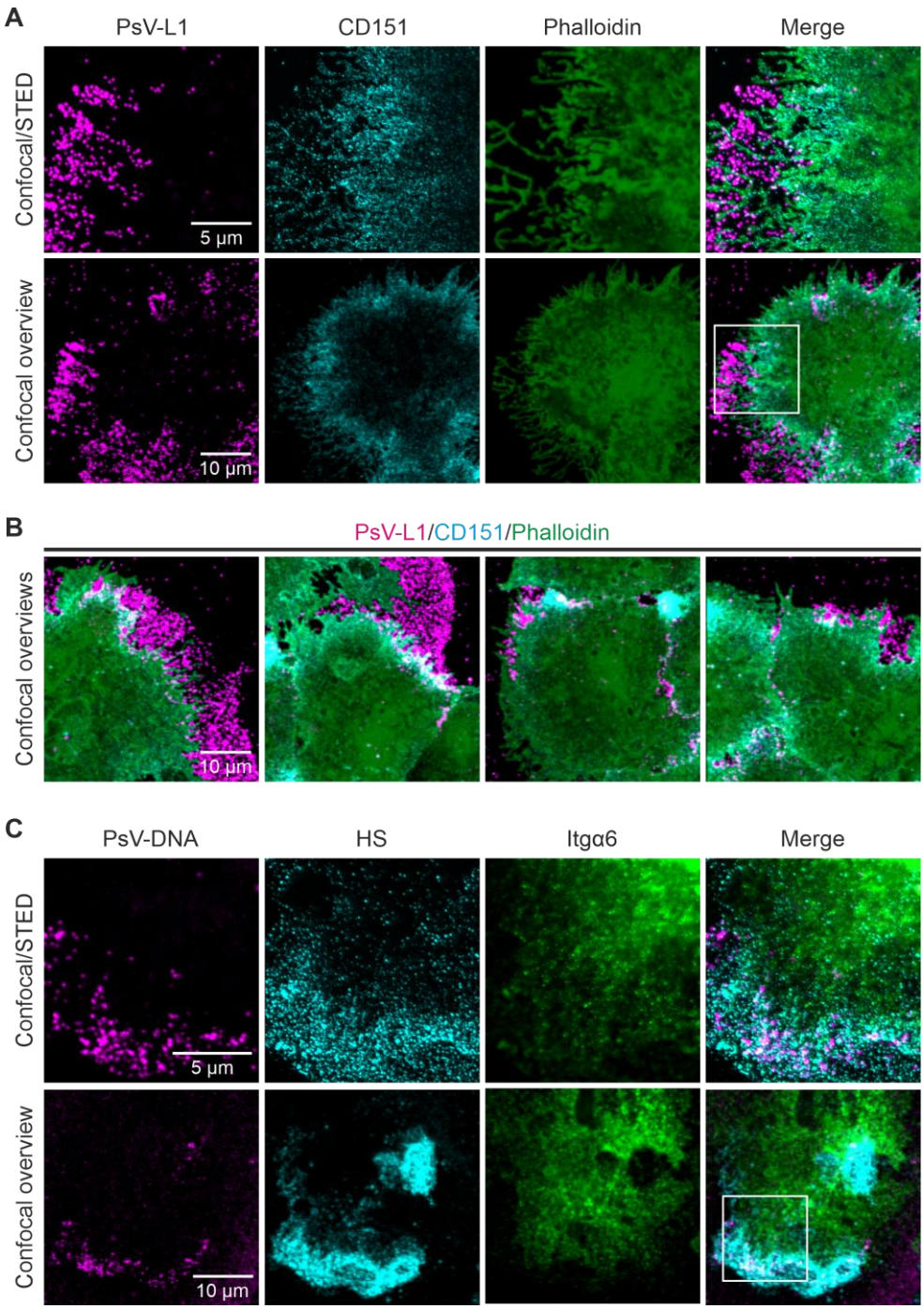

Supplementary Figure 3. *Overview images.*
(A) Upper row, micrographs shown in Figure 5A, CytD/0min, using for CD151 a cyan instead of a green LUT, and showing as well F-actin staining (green LUT). Lower row, confocal overview images. After taking the overview images, the area in the white box was imaged as described in the legend of Figure 5, yielding the images shown in the upper row. (B) More merged overview images from the experiment described in Figure 5, condition CytD/0 min, showing examples of large and small PsV accumulations. (C) Upper row, same micrographs as shown in Figure 6A, CytD/0 min. Lower row, confocal overview images. The area in the white box was imaged as described in the legend of Figure 6, yielding the images of the upper row in C.

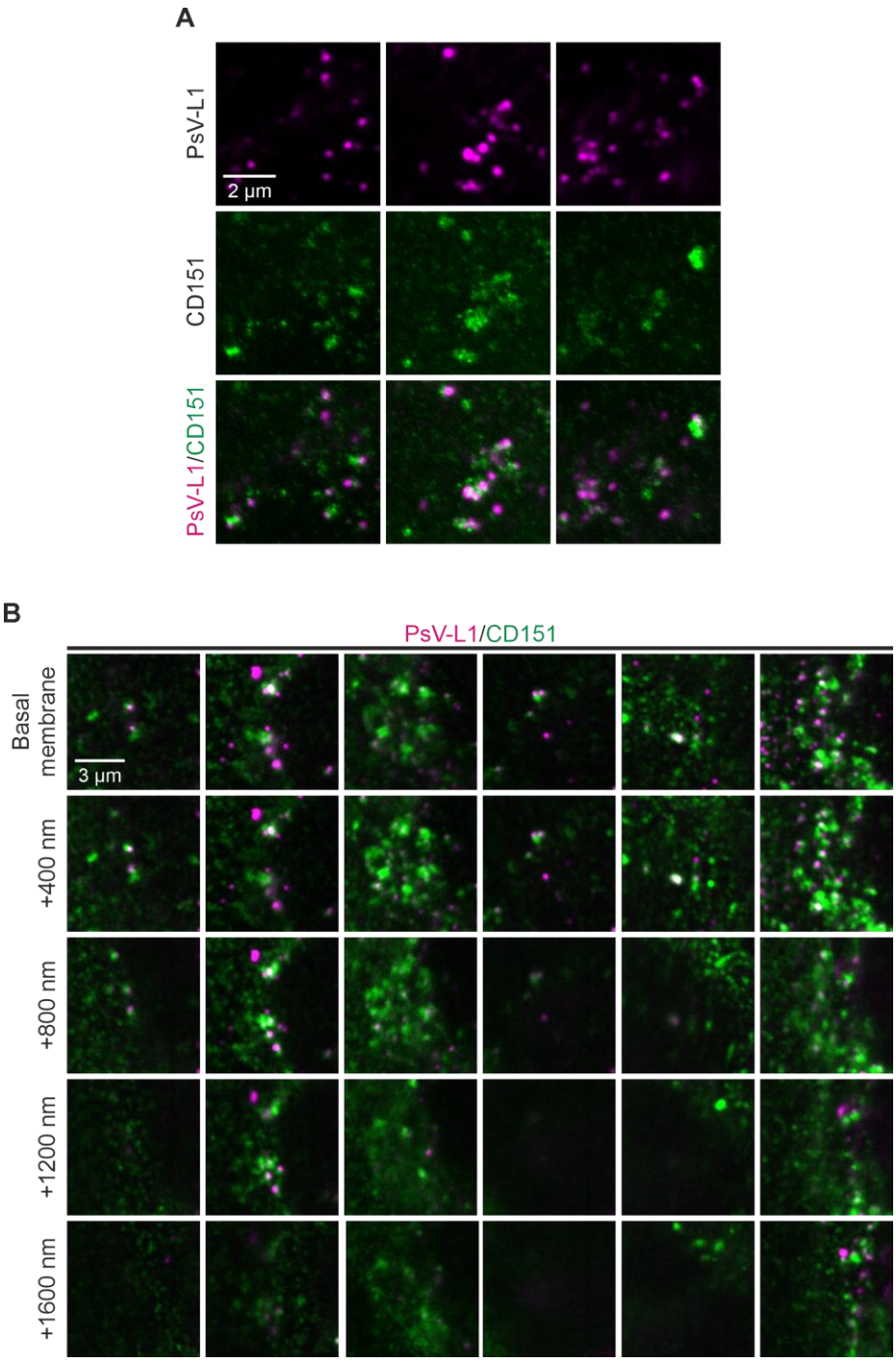

1312

1313 **Supplementary Figure 4.** *Examples of agglomerated CD151 maxima associated with PsVs that*
1314 *presumably represent endocytic structures.*
1315 (A) From the CytD/180 min time point described in Figure 5, we show more examples of agglomerated
1316 CD151 maxima (green LUT, see green patches) that associate with PsVs (magenta LUT). (B) Same
1317 experiment as in (A). Starting at the basal membrane, at confocal resolution we imaged CD151 (green
1318 LUT) and PsV-L1 (magenta LUT). Cells were further scanned by 400 nm steps in the axial direction.
1319 Some of the CD151 agglomerates noticed in the basal membranes appear to continue deeper into the
1320 cell, in the second example from the left more than a micrometer. We propose that the agglomerated
1321 CD151 maxima that overlap with PsVs are endocytic structures, as CD151 has been shown to co-
1322 internalize with PsVs (***Scheffer et al., 2013***), and as these structures invaginate into the cell, like PsV
1323 filled tubular organelles previously described by electron microscopy (***Schelhaas et al., 2012***). Images

in (A) and (B) are shown at the same settings of brightness and contrast but at different settings compared to Figure 5.

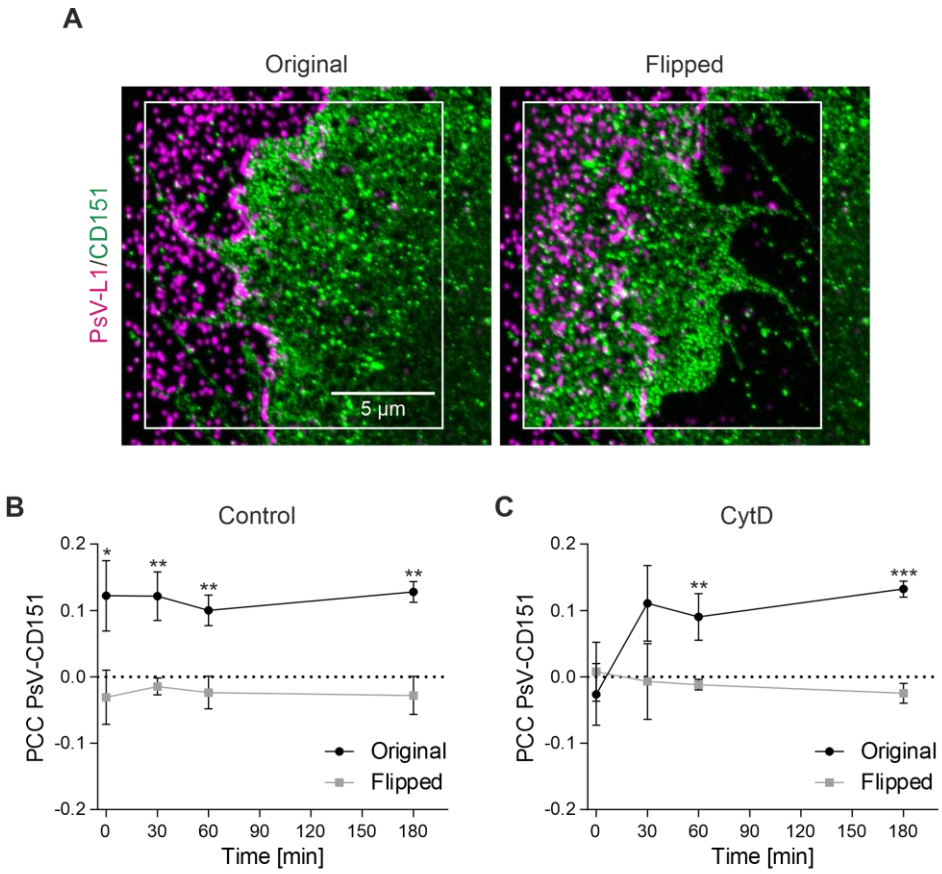

Supplementary Figure 5. *PCC values of flipped images.*
(A) For each image pair, we determined the PCC on non-overlapping images with the same density of objects and intensities. To this end, one channel was flipped horizontally and vertically. Left, original images (from the CytD/0 min condition). The ROI for analysis is illustrated as white box. Right, in the ROI, the CD151 image (green LUT) was flipped horizontally and vertically. (B + C) Shown are again the PCCs over time of Figure 5C of the original images ((B) Control, (C) CytD) together with the PCCs of the respective flipped images. Values are given as means ± SD (n = 3 biological replicates). Statistical differences between the same time points of original and flipped images was analyzed by using the two-tailed, unpaired student's *t*-test (n = 3, for details see methods).

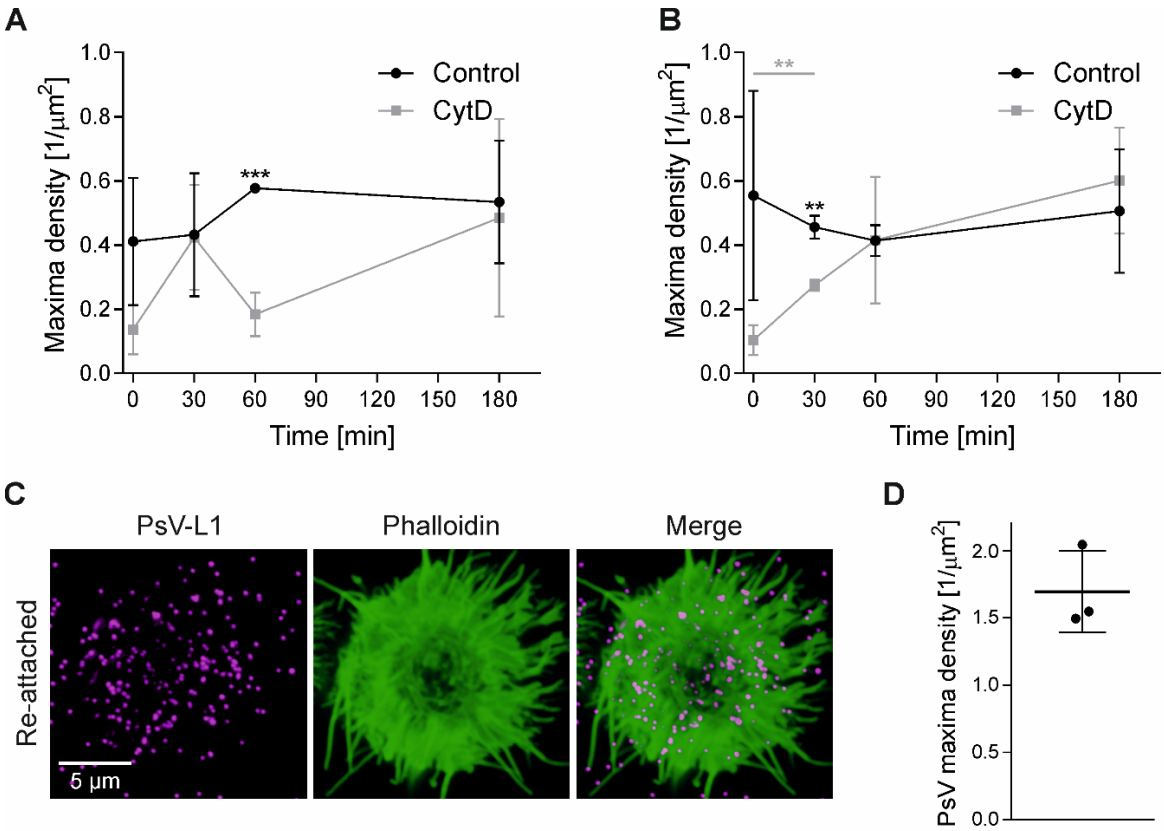

Supplementary Figure 6. *PsV density at the membrane of normally grown and re-attached HaCaT cells.* (A + B) In order to count the PsVs at the basal membrane of the experiments shown in (A) Figure 5 (PsVs visualized by antibody labeling) and (B) Figure 6 (PsVs visualized by click-chemistry), we placed ROIs covering only the cell body. Within these ROIs the PsV maxima were counted and related to the size of the analyzed area. Values are given as means ± SD (n = 3 biological replicates). Statistical differences between Control and CytD at each time point were analyzed by using the two-tailed, unpaired student's *t*-test (n = 3, for details see methods). (C) HaCaT cells were detached by a 15 min incubation with 10 mM EDTA (in PBS) and incubated with PsVs at 4 °C for 1 h under constant rotation. After washing the cells three times with PBS, they were seeded onto PLL-coated glass coverslips for 1 h. Then, cells were washed, fixed and stained for L1 (STAR GREEN; magenta LUT) by indirect immunofluorescence and for F-actin by iFluor647-labelled phalloidin (green LUT). PsV-L1 and F-actin staining were imaged as in Figure 5 in the confocal mode of a STED microscope. (D) Analysis as in (A + B). Values are given as means ± SD (n = 3 biological replicates).

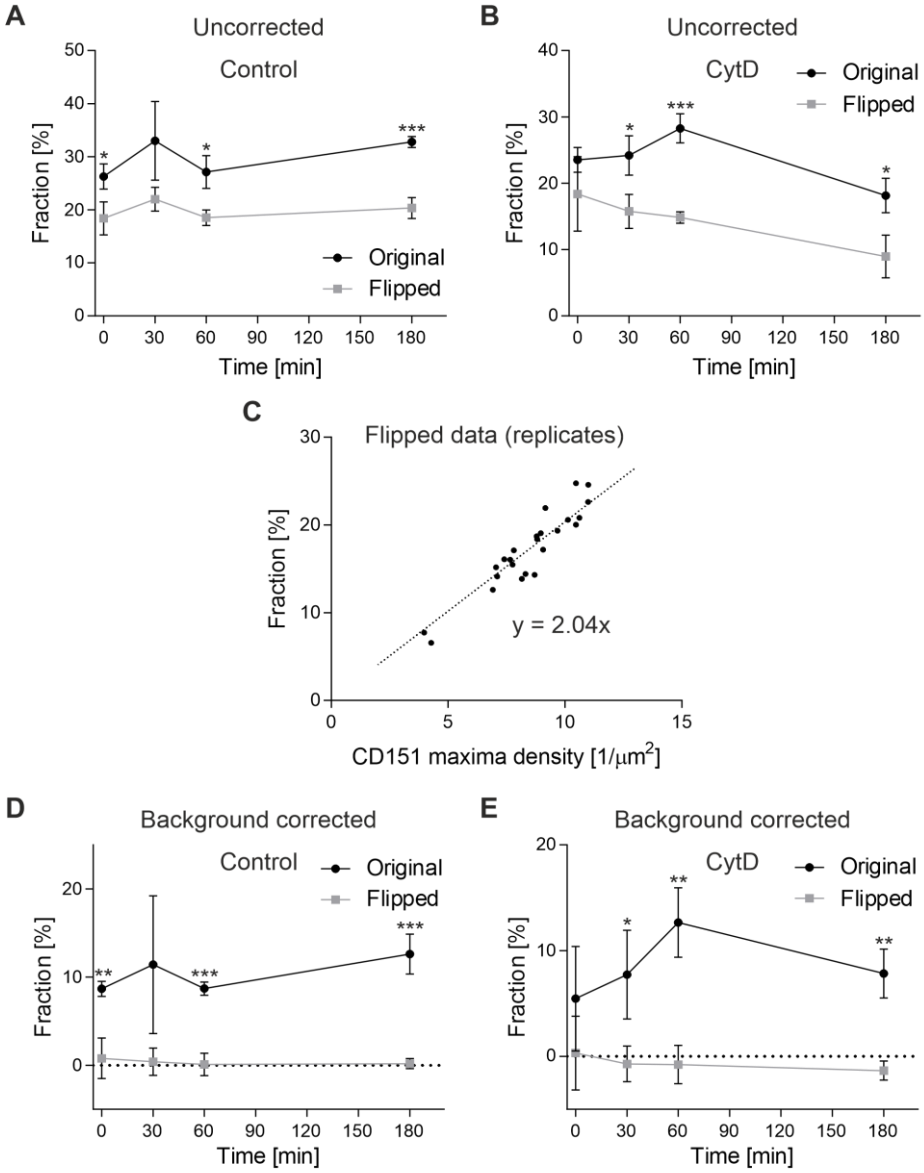

Supplementary Figure 7. *Background correction of the fraction of PsVs closely associated with CD151.* (A) The fraction of closely associated PsVs (PsV-L1 maxima with a distance ≤ 80 nm to the next nearest CD151 maximum) in the Control of Figure 5 was analyzed on original and flipped images (for an example of a flipped image see Supplementary Figure 5A). As shown in (A), on flipped images, we often find values more than half of the values of the original images, demonstrating that many PsVs have a distance ≤ 80 nm to CD151 merely by chance, in the following referred to as background association. (B) Same as (A), for CytD. (C) The value of each time point in (A) and (B) is the average of three biological replicates. We take the altogether 24 fraction values obtained on flipped images (12 values from Control and CytD each), and plot the fraction of closely associated PsVs against the average CD151 maxima density in the respective images. As can be seen in (C), the fraction increases with the maxima density, as the chance of a distance ≤ 80 nm increases with the maxima density. The fitted linear regression line describes how the background association depends from the maxima density. As a result, the background association (y) can be calculated for any maxima density (x) with the equation y = 2.04 • x. The CytD/0 min condition may be overcorrected, if it includes many images with CD151 flipped onto peripheral PsVs that actually are distal to CD151 (for an example ROI see Supplementary Figure 5A). On the other hand, PsVs right at the cell border, where CD151 staining

1374 tends to be strong (Supplementary Figure 5A), after flipping have less CD151 than before, contributing
1375 to undercorrection. (D) and (E), for each original and flipped replicate included in (A) and (B), the
1376 background was calculated using the above equation and subtracted from the uncorrected value. The
1377 average original background corrected values are shown in Figure 5D. Values are given as means ± SD
1378 (n = 3 biological replicates). Statistical differences between the same time points of original and flipped
1379 images were analyzed by using the two-tailed, unpaired student's *t*-test (n = 3, for details see
1380 methods).

1381
1382

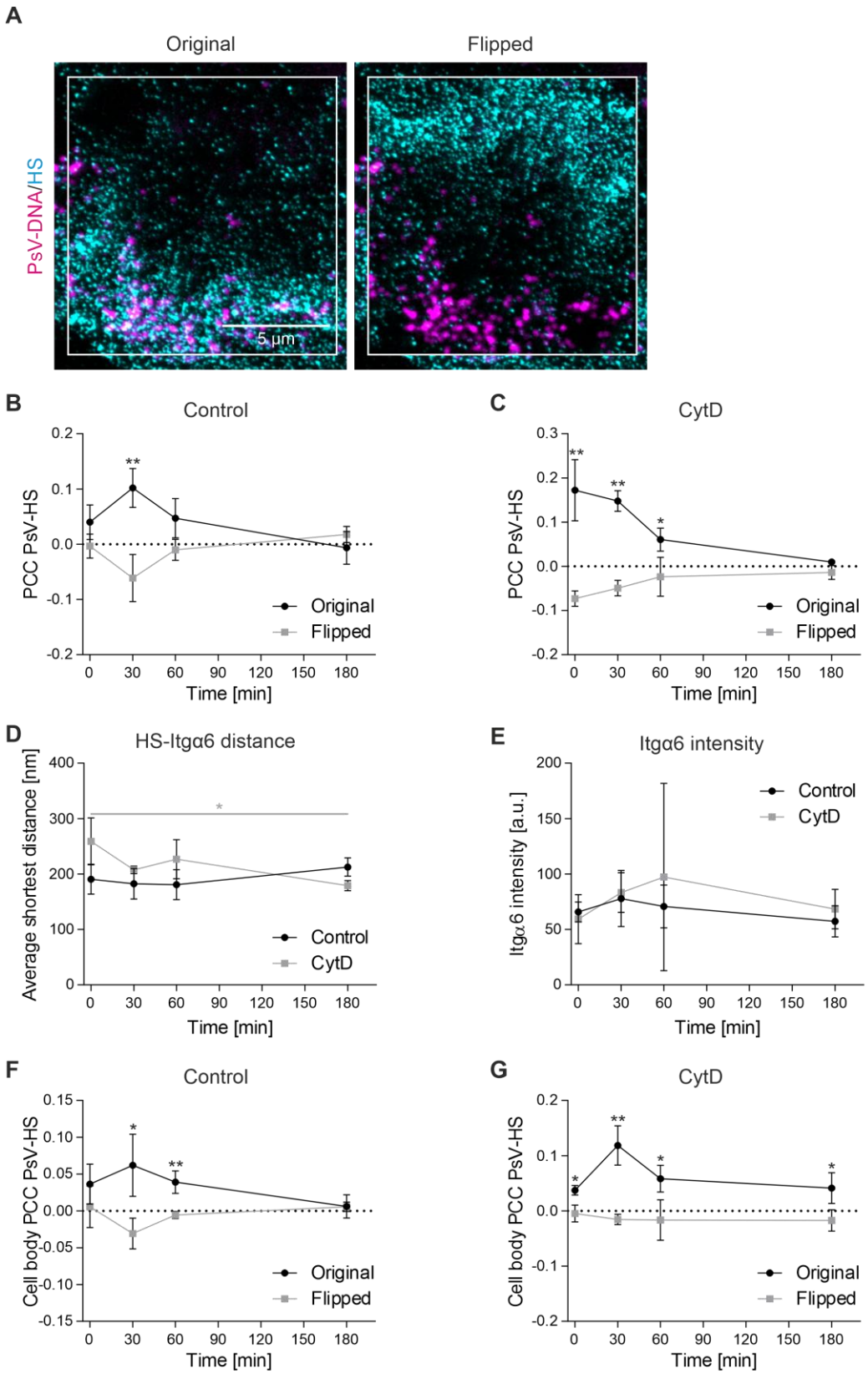

Supplementary Figure 8. *PCC values of flipped images, HS-Itgα6 shortest distance and Itgα6 intensity.* (A) For each image pair, we determined the PCC on respective non-overlapping images with the same density of objects and intensities. To this end, one channel was flipped horizontally and vertically. Left, original images (from the CytD/0 min condition). The ROI for analysis is illustrated as white box. Right, in the ROI, the HS image (cyan LUT) was flipped horizontally and vertically. (B + C) Shown are the PCCs

1389 over time of Figure 6C obtained with the original images ((B) Control, (C) CytD) together with the PCCs
1390 of the flipped images. (D) The shortest distance of HS maxima to the next nearest Itgα6 maxima over
1391 time. (E) The mean Itgα6 intensity over time. (F + G) Shown are the PCCs over time of Figure 6D
1392 obtained with the original images ((F) Control, (G) CytD) together with the PCCs of the flipped images.
1393 Values are given as means ± SD (n = 3 biological replicates). Statistical differences between the same
1394 time points of original and flipped image ((B), (C), (E), (F) and (G)) or between CytD/0 min and
1395 CytD/180 min (D) were analyzed by using the two-tailed, unpaired student's *t*-test (n = 3, for details
1396 see methods).
1397

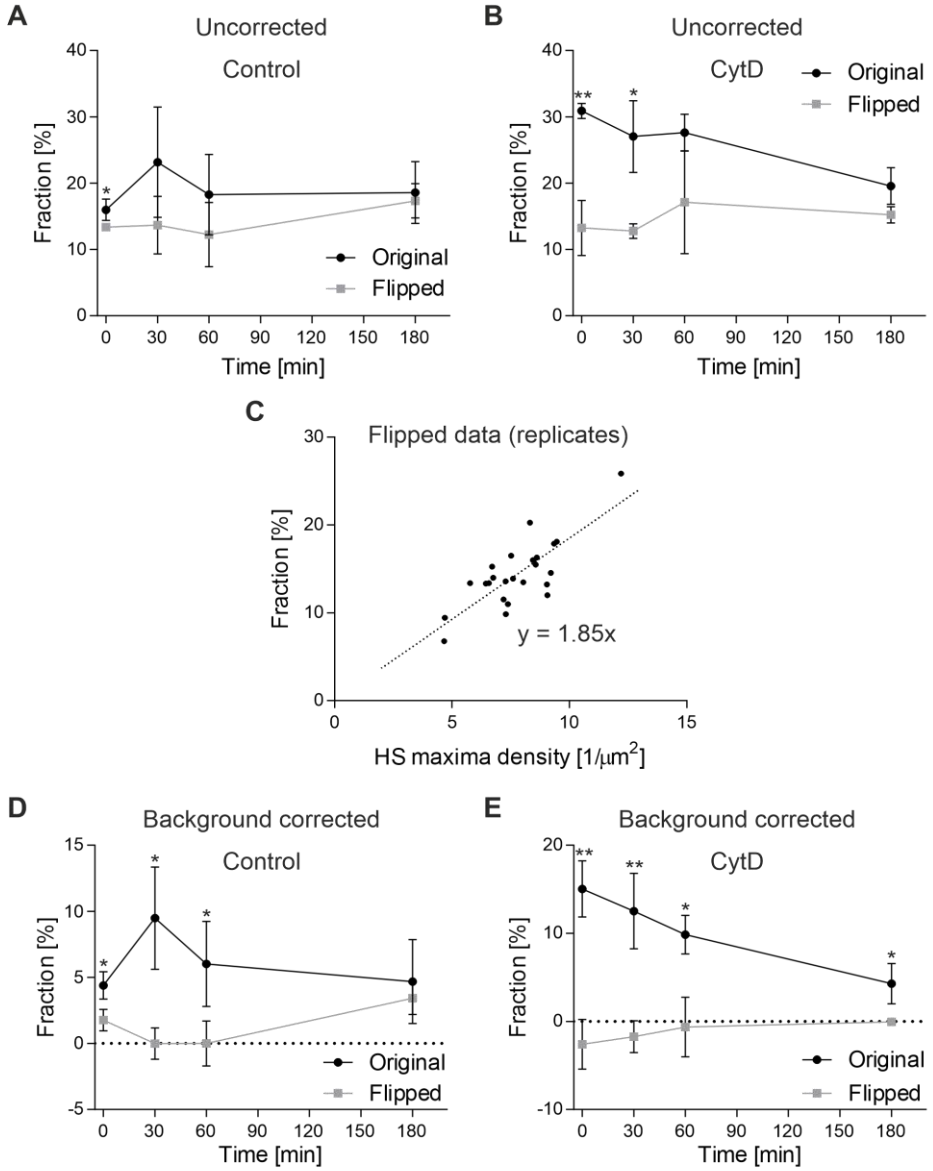

Supplementary Figure 9. *Background correction of the fraction of PsVs closely associated with HS.* (A) The fraction of closely associated PsVs (PsV-DNA maxima with a distance ≤ 80 nm to the next nearest HS maximum) in the Control of Figure 6 was analyzed on original and flipped images (for an example of a flipped image see Supplementary Figure 8A). (B) Same as (A), for CytD. (C) From the altogether 24 fraction values obtained on flipped images (12 values from Control and CytD each), we obtain the equation y = 1.85 • x for calculating the background association (please see Supplementary Figure 7 for more details). (D) and (E), for each original and flipped replicate included in (A) and (B), the background was calculated using the above equation and subtracted from the uncorrected value. The average original background corrected values are shown in Figure 6E. Values are given as means ± SD (n = 3 biological replicates). Statistical differences between the same time points of original and flipped images were analyzed by using the two-tailed, unpaired student's *t*-test (n = 3, for details see methods).

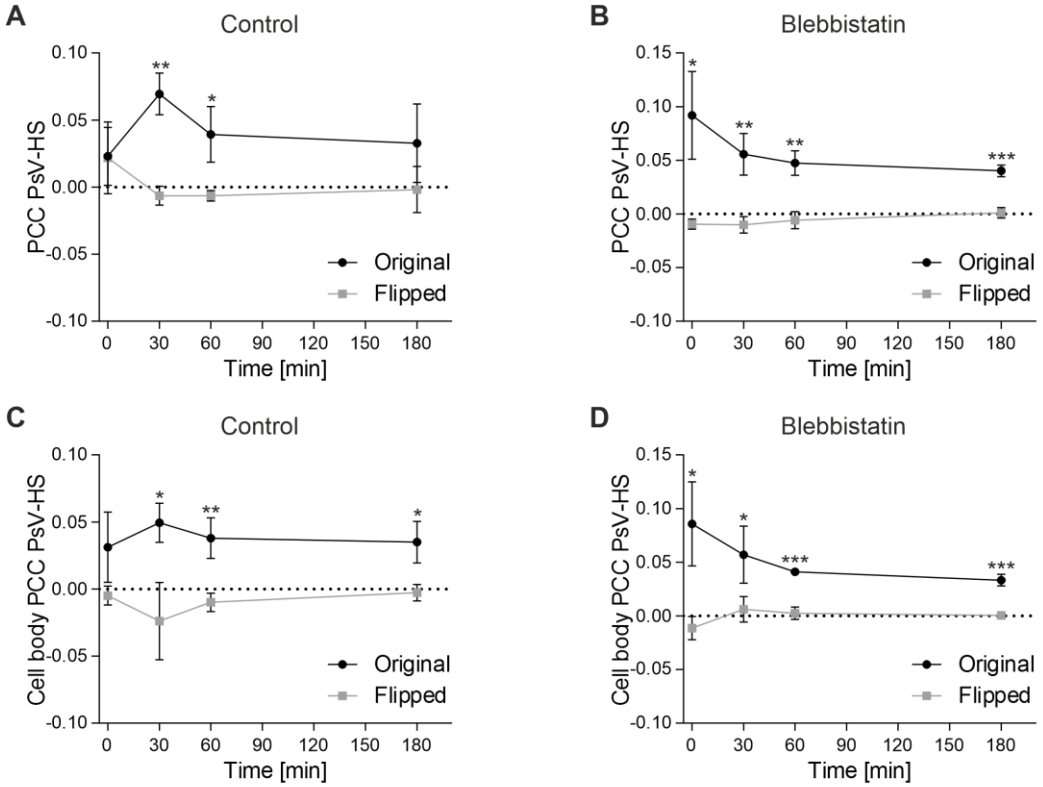

Supplementary Figure 10. *PCC values of flipped images.*
(A) and (B) The PCC values between PsV and HS of Figure 8C ((A) Control, (B) Blebbistatin) plotted together with the respective PCC values of flipped images. (C) and (D) The cell body PCC values between PsV and HS of Figure 8D ((C) Control, (D) Blebbistatin) plotted together with the respective PCC values of flipped images. Values are given as means ± SD (n = 3 biological replicates). Statistical differences between the same time points of original and flipped images were analyzed using the two-tailed, unpaired student's *t*-test (n = 3, for details see methods).

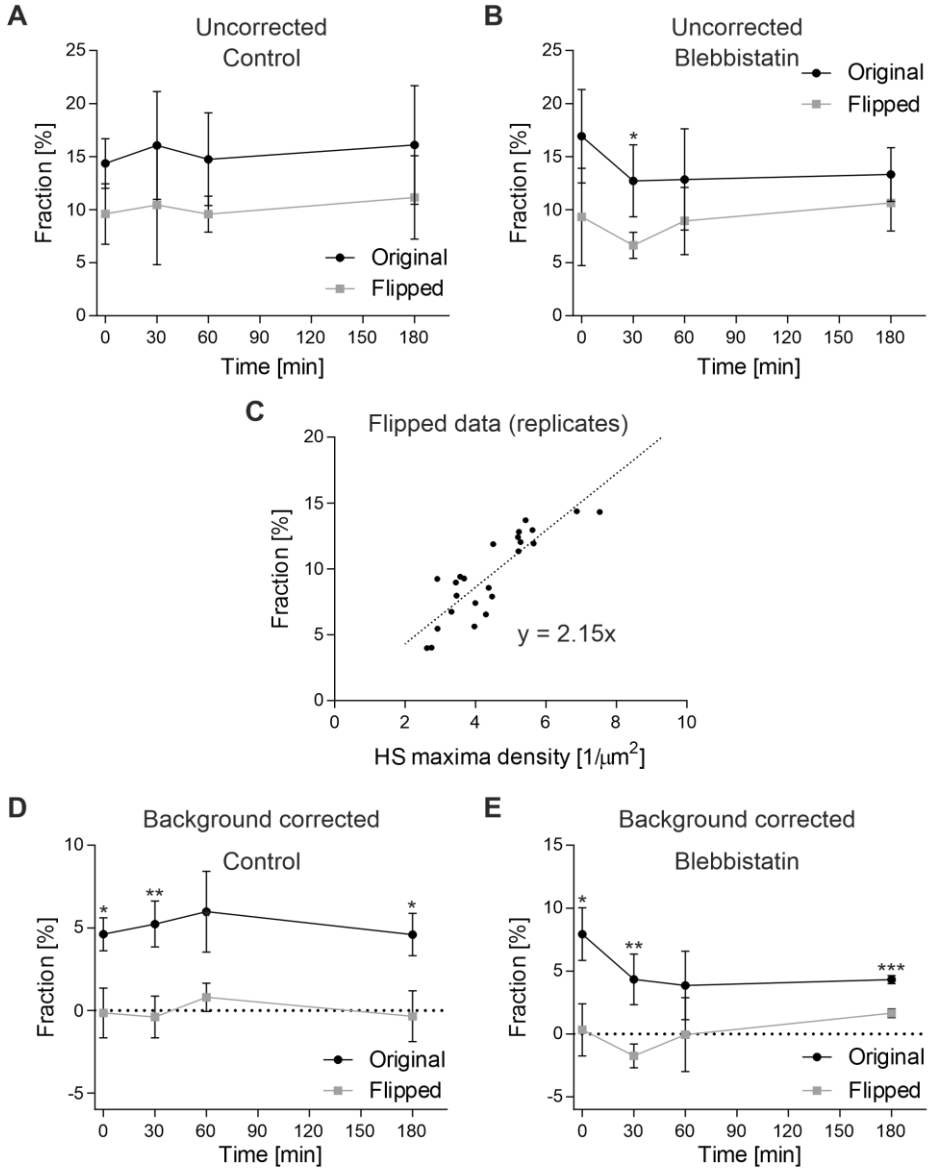

Supplementary Figure 11. *Background correction of the fraction of PsVs closely associated with HS after blebbistatin treatment.*

(A) The fraction of closely associated PsVs (PsV-L1 maxima with a distance ≤ 80 nm to the next nearest HS maximum) in the Control of Figure 8 was analyzed on original and flipped images. (B) Same as (A), for blebbistatin. (C) From the altogether 24 fraction values obtained on flipped images (12 values from Control and Blebbistatin each), we obtain the equation y = 2.15 • x for calculating the background association (please see Supplementary Figure 7 for more details). (D) and (E), for each original and flipped replicate included in (A) and (B), the background was calculated using the above equation and subtracted from the uncorrected value. The average original background corrected values are shown in Figure 8E. Values are given as means ± SD (n = 3 biological replicates). Statistical differences between the same time points of original and flipped images were analyzed by using the two-tailed, unpaired student's *t*-test (n = 3, for details see methods).

Supplementary Table 1. Fraction of PsVs in percent of each of the four distance categories (see left column). Values are means ± SD of the data shown in Figure 7B. For each time point and category, p-values between Control and CytD were calculated by using the two-tailed, unpaired student's *t*-test (n = 3 biological replicates). P-values < 0.05 are illustrated in bold.

	0 min			**30 min**			**60 min**			**180 min**		
	Control [%]	CytD [%]	p-value	Control [%]	CytD [%]	p-value	Control [%]	CytD [%]	p-value	Control [%]	CytD [%]	p-value
HS < 250 nm & ltgα6 < 250 nm	62.31 ± 5.05	47.83 ±3.26	**0.0271**	65.48 ± 8.35	63.67 ± 1.14	0.7764	59.06 ± 10.64	67.16 ± 9.84	0.4739	63.69 ± 4.27	59.28 ± 3.17	0.3065
HS < 250 nm & ltgα6 > 250 nm	12.18 ± 5.51	46.04 ± 3.67	**0.0019**	15.46 ± 3.14	26.12 ± 2.16	**0.0167**	13.25 ± 1.94	19.87 ± 3.12	0.0637	11.97 ± 1.53	10.64 ± 1.15	0.3808
HS > 250 nm & ltgα6 < 250 nm	21.59 ± 4.07	4.34 ± 0.37	**0.0040**	15.83 ± 5.73	8.58 ± 2.33	0.1723	23.49 ± 6.55	9.60 ± 4.81	0.0731	20.88 ± 3.31	25.24 ± 1.96	0.1842
HS > 250 nm & ltgα6 > 250 nm	3.93 ± 0.30	1.79 ± 0.60	**0.0110**	3.23 ± 0.88	1.63 ± 0.21	0.0675	4.19 ± 2.43	3.38 ± 2.20	0.7425	3.46 ± 0.54	4.84 ± 2.87	0.5393